Simulation of the Mechanical Behaviour of Low Density Paper and an Individual Inter-fibre Bond

by

Majid Targhagh

B.Sc., Amirkabir University of Technology (AUT), 2013

A THESIS SUBMITTED IN PARTIAL FULFILLMENT OF
THE REQUIREMENTS FOR THE DEGREE OF

MASTER OF APPLIED SCIENCE

in

THE COLLEGE OF GRADUATE STUDIES

(Mechanical Engineering)

THE UNIVERSITY OF BRITISH COLUMBIA

(Okanagan)

May 2016

The undersigned certify that they have read, and recommend to the College of Graduate Studies for acceptance, a thesis entitled:

Simulation of the Mechanical Behaviour of Low Density Paper and Individual Inter-fibre Bond

Submitted by Majid Targhagh in partial fulfillment of the requirements of

The degree of Master of Applied Science .

Dr. Andre Phillion, School of Engineering, UBCO
Supervisor, Professor (please print name and faculty/school above the line)

Dr. Abbas Milani, School of Engineering, UBCO
Supervisory Committee Member, Professor (please print name and faculty/school in the line above)

Dr. Joshua Brinkerhoff, School of Engineering, UBCO
Supervisory Committee Member, Professor (please print name and faculty/school in the line above)

Dr. Goran Fernlund, Composites Materials Engineering, UBC Vancouver
University Examiner, Professor (please print name and faculty/school in the line above)

May 10, 2016
(Date submitted to Grad Studies)

Abstract

The strength of paper is a multi-scale problem. Although paper is a thin product, its strength depends on the characteristics of the microstructure in the thickness direction as well as the orientation of each fiber. Characterizing the effect of these morphological properties of the papermaking fibres on the strength of paper is a vital step in understanding the behaviour of paper handsheets. Numerical simulation methods, such as the Finite Element Method (FEM) enable us to simulate the mechanical behaviour of paper using the actual geometry of the papermaking fibres.

In this work, two groups of FE simulations were performed to study the pre-failure behaviour of an individual inter-fibre bond as well as the response of the low density paper geometries, formed based on the Northern Bleached Softwood Kraft (NBSK) fibres, to uni-axial tensile deformation. The simulation geometries were formed based on the actual geometry of the NBSK fibres that were extracted from the μCT scan of the paper handsheets,

The results of the simulations were used to study the effect of the morphological properties of NBSK fibres such as length and diameter on the peeling strength of the bond, and the effect of the properties of the geometry, such as basis weight, mixture of hardwood and softwood fibres, and length and thickness of the NBSK fibres, on the tensile index of the geometry. These results showed that the simulation geometries with a higher basis weight and smaller fibre's elastic modulus lead to a lower tensile index. Further, it is shown that the increase in the softwood content of the hardwood/softwood mixed geometries increased the bulk tensile index of paper. Finally, the results of the tensile strength simulations were compared to the results of the experimental tensile strength tests that were performed on the actual paper handsheets. The results of these simulations provide a new insight into the mechanical behaviour of paper and interaction of fibres under deformation of paper.

Preface

This work has been done at UBC's Okanagan campus under the supervision of Dr. Andre Phillion and Dr. Mark Martinez. With the exception of my supervisors, who provided detailed suggestions on the simulations and analytical analysis, I am the primary contributor of the work.

In Chapter 4, I have presented the results of the FE simulations. The images of the NBSK fibres that were used to develop the 3D mesh of the fibres were provided by Yash Sharma. The 3D mesh was developed in the Solidification Processing and Simulation Laboratory (SPSL) at UBC Okanagan campus.

In Chapter 4, I have also presented the artificial fibre generation script that was used to generate simulation geometries for the tensile strength simulations. This script was developed based on a preliminary code that was written by Pouyan Jahangiri to place cylindrical fibres in a blank volume.

In Chapter 5, the results of the Finite Element (FE) simulations are presented. I have presented part of the results of the simulations of the behaviour of an individual inter-fibre bond at the International Conference of Mechanics of Complex Solids and Fluids (ICMCSF), Lille, France, 2015.

Table of Contents

List of Tables

List of Figures

Acknowledgements

I am gratefully thankful to my supervisor Prof. Andre Phillion, for his mentorship and support during this project. He has been always there for me in both academic and non-academic matters. Thanks to his guidance, I grew as a researcher and improved my presentation skills. I would also like to thank all of the members of SPSL research group for creating a positive atmosphere in the group and imaging laboratory.

I would like to express my sincere thanks to my co-supervisor Prof. Mark Martinez, for his encouragement and insights. His constant guidance helped me to expand my knowledge about pulp and paper and develop and develop a practical research project.

I wish to acknowledge the work of Yash Sharma, for providing the tomography scanned images of paper samples. The results of his work were very helpful in creating the Finite Element simulations. I am also grateful to my colleague and friend, Pouyan Jahangiri. His initial efforts in generating a random network of fibres were vital in defining the objective of this research.

I offer my gratitude to Moein Ahmadipour, Sadegh Hasanpour, Sepehr Zarifmansour, Nima Moallemi, Sadaf Moallemipour, Farzin Golkhosh, Mahsa Haghjoo, and Shelir Ebrahimi who made my stay in Canada enjoyable.

Special thanks are owed to my parents and brother, whose have supported me throughout my years of education, both morally and financially. It was under their watchful eye that I gained so much drive and ability to tackle the challenges ahead. They have helped me to start a new life in a new country and that means a world to me.

Finally, I would like to acknowledge the financial support of Natural science and Engineering Research Council (NSERC) and Canfor Corporation.

To my beloved parents

Hassan and Fariba

Chapter 1: Introduction

1.1 General Remarks

The pulp and paper industry is one of the most important elements of Canada's economy, especially in the province of British Columbia. With over 50 percent of the land mass of the country covered by forests, Canada contains 10 percent of the world's forest resources. Due to the environmental factors relating to the growing conditions of spruce, fir, and pine trees, as well as substantial research and funding, Canada remains the world's largest producer of newsprint and Northern Bleached Softwood Kraft (NBSK) pulp [1]. Although the main function of paper is the absorption of the printing liquid, it is also necessary that it withstand the mechanical loads to which it is subjected when in use. New advances in the papermaking process require new understanding of deformation mechanisms within paper. This can be studied by different methods based on experimental testing and numerical simulation. When creating numerical models, it is often difficult to create a geometry/mesh that closely matches the real structure of fibrous materials. Using new imaging methods, such as X-ray Computed Tomography (CT), in combination with new image-based modelling techniques, the real morphology of papermaking fibres can be meshed and used in the numerical simulations. This combination of techniques also allows the effect of mixture rules on mechanical behaviour to be studied in a systematic fashion.

1.2 Pulping and Paper Making

Paper production is a multi-stage process, starting with the selection of the tree types in the forest and finishing with paper at the paper machine. Once the wood is harvested, the process can be separated into two major stages: pulping and papermaking. The pulping process converts the wood into an aqueous solution of papermaking fibres, i.e. pulp. The paper machine then converts the pulp into a thin sheet of paper as the final product. Two major types of trees are often used to produce paper, hardwoods and softwoods. Figure 1.1 shows the microstructure of each type. Softwoods are conifer trees that do not lose their green needles during the winter; some of the best know members of this type are pines, spruces, firs, and hemlocks. Softwood fibres have thin walls and an average fibre length of 3 mm, which provides additional strength for the final product, such as shipping containers and writing paper [2]. Hardwoods are mostly flowering plants with broad leaves, such as maple, birch, and oak. Hardwood fibres, in contrast to softwoods have relatively thicker walls and an average fibre length of 1 mm [2].

(a)

(b)

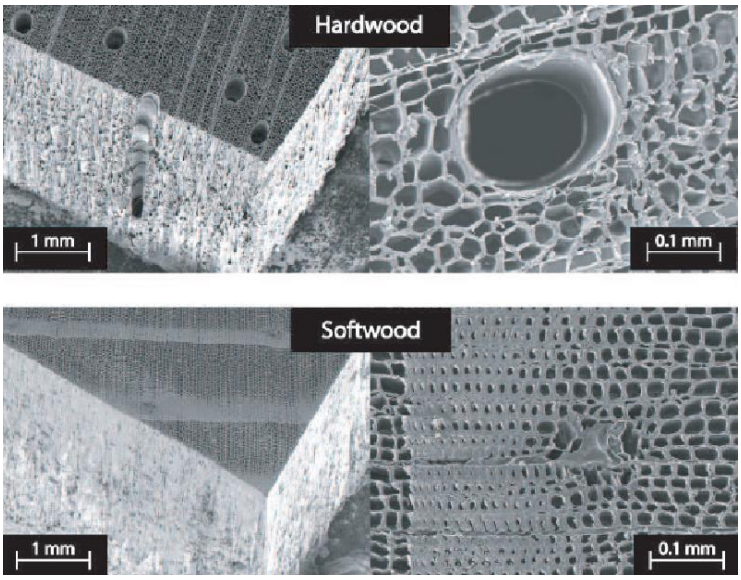

Figure 1.1 - Typical microstructure of the cross section of paper a) Hardwood trees, b) Softwood trees [3]

Northern Bleached Softwood Kraft (NBSK) is a benchmark grade of pulp that is produced in significant quantities in Canada. NBSK from British Columbia is mainly from Lodgepole Pine, with a significant amount of White Spruce [4]. NBSK is known for having longer fibre lengths and larger fibre diameters, therefore, it is used as the reinforcement in softwood/hardwood mixtures and also for producing tissue paper [5].

Hardwood and softwood fibres can be blended into a single paper to achieve a desired combination of strength, whiteness, writing surface and/or other required characteristics e.g. tissue. In order to study the strength of paper resulting from this mixture, it is necessary to study the behaviour of the papermaking fibres at the network/microstructure level.

1.3 Finite Element Analysis (FEA)

Finite Element Analysis (FEA) has become commonplace in recent years and is now the basis for simulating mechanical deformation. FEA is a numerical technique that gives an approximate solution to the differential equations that represent engineering problems. Commercial FE packages, such as Abaqus™, are widely used to simulate the mechanical behaviour of engineering materials.

In practice, a finite element -based simulation usually consists of three principal stages:

1. **Preprocessing:** The user constructs a model of the part to be analyzed. As with other numerical schemes, FEA requires the partitioning of a geometrical domain into smaller volumes known as *elements*, each connected to discrete points called *nodes*. Particular boundary conditions are then applied to some of these nodes that have fixed displacements, while others have prescribed loads.
2. **Analysis:** The preprocessing dataset is used as the input of the finite element code, which constructs and solves a set of algebraic equations for the deformation of the nodes. In a general FE analysis, the deformation of individual nodes is calculated based on the boundary conditions/applied forces and the material properties of the geometry. The general form of the equation of the deformation of a node is shown in equation 1.1.

   $$K_{ij}u_{ij} = f_i \tag{1.1}$$

   where **u** and **f** are the displacement and externally applied forces at the nodal points, **K** is the "Stiffness Matrix", containing information regarding the material properties, geometry, and loads and parts, and **i** and **j** are counters indicating node numbers.

   The deformation equations for all of the nodes are then assembled and solved in matrix form to find the total displacement of the part. The solution can then be used to determine the local deformations of the nodes and the resulting stresses within a component.
3. **Post processing:** In this stage, the user analyzes the results, such as principal stresses, displacements, amongst others, through the meshed geometry. Since errors in the input data can cause widely incorrect results, the calculated values need to be carefully examined, and verified against experimental or reference data.

FEA is extensively used for solving general stress and damage problems in mechanical engineering and structural analysis. This method is particularly well suited to study the constitutive behaviour of complex geometries such as composite materials and fibrous structures. As mentioned above, paper is a composite material consisting of a random network of fibres and voids/air that shows a very complex response to the applied loading. FEA is thus well suited to simulate the constitutive behaviour of paper products to investigate the deformation mechanisms of the paper products at the microstructure level.

1.1 Summary

There is industrial need to understand the strengthening parameters of paper products generated based on NBSK fibres. Studying the deformation behaviour of the microstructure of paper at the fibre level will provide new insights into the mechanics of paper, In this thesis, numerical simulations are combined with 3D imaging to simulate the mechanical behaviour of an individual inter-fibre bond as well as the bulk mechanical behaviour of paper geometries that were formed from the actual geometry of the NBSK fibres. These new 3D deformation simulations provide detailed information about the deformation and failure of the fibres in the microstructure of paper, and also provide a better understanding of the experimental tensile strength test results found in the literature.

This project is performed in collaboration with UBC's Pulp and Paper Center (PPC) and Canfor Corporation to establish a knowledge base in simulating the behaviour of paper and papermaking fibres using their actual geometry. The knowledge gained from this research will provide Canfor Corporation with a better understanding of the behaviour of paper at the microscale level as well as a link between the morphology of fibres and the bulk constitutive properties of paper. Further, this research will help the company to determine the proper type/mixture of fibres to produce an improved paper handsheet with a higher rupture index.

Chapter 2: Literature review

2.1 Overview

Paper is a versatile material that has been used for many years for different purposes, such as filters, electrical insulators, and publications. Although the production process is mature, there is considerable interest in developing a better understanding of the process-structure-manufacturing relationship to allow for the creation of better paper products. For instance, the mechanical properties of paper are highly dependent on the process of Low Consistency refining, with higher energy input leading to higher paper strength. This makes profits in the paper market industry vulnerable to energy costs and availability. Thus, there is strong incentive to invest in research that improves the pulp and papermaking process [6]. A measure to streamline this process is to use numerical methods such as Finite Element (FE) to model the mechanical behaviour of paper. Numerical simulations can be easily repeated multiple times and would remove many costly and tedious experimental tests. In order to simulate the behaviour of paper, a geometrical mesh and a constitutive mechanical model are necessary. This chapter provides a survey on previous research that has been done to build a basis for this purpose.

As an introduction for the FE simulations, the physics of paper are described in section 2.2. The mechanical properties of paper, and the pulp and paper terms that are used in this thesis are explained in section 2.3. A review of methods for experimental testing of the strength of paper is highlighted in section 2.4. Recent progress made to model the behaviour of fibrous materials, especially the models that are used to describe the tensile strength of paper, is presented in section 2.5. Section 2.6 highlights some of the previous numerical simulations that have been used to study the behaviour of paper including both elastic and elastic-plastic behaviour along with failure analysis. A short review on the previous studies of mechanical behaviour of an individual inter-fibre bond in paper are presented in section 2.7. Finally, the recent studies on the strength of the inter-fibre bonds in paper and the imaging techniques that are used for visualizing the structure of paper are discussed in section 2.8 and 2.9.

2.2 Physics of paper

2.2.1 Production process

In order to produce paper, wood chips and other materials are diluted into a solution of water known as pulp. The pulping process breaks down the structure of wood by means of chemicals or mechanical grinders [7, 2, 8]. The pulp, which consists of 99 percent water, is then drained with a wire web to aggregate and sediment the papermaking fibres. In the next step, the network of fibres is pressed and dewatered between rolling cylinders that are heated with steam. During the pressing step, 90 % of the water content is removed, increasing the solid content of the paper from 10 to 91-95 % [9, 10, 6]. The drainage direction has a significant effect on the final product's mechanical properties. Most of the fibres become aligned in a direction parallel to the paper machine, a direction known as the "Machine Direction" (MD). The other two directions are known as "Cross Direction" (CD; perpendicular in-plane), and "Thickness Direction (TD, perpendicular out-of-plane), respectively, as illustrated in Figure 2.1. This alignment results in anisotropic mechanical properties of the final paper sheet and a considerably higher stiffness in the machine direction.

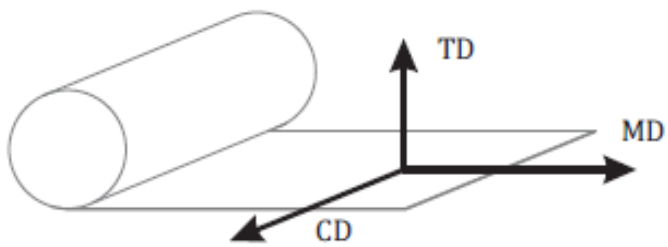

Figure 2.1 - Illustration of the principle directions of pulp [6]

2.2.2 Microstructure of paper

A 3D image of the microstructure of paper scanned using X-ray micro tomography is shown in Figure 2.2. A typical sheet of paper has, in general, ten fibres in the thickness direction. The length of most of the fibres is more than ten times larger than the sample's thickness [11]. As can be seen in the figure, the microstructure of paper consists of a complex network of hollow cellulose based cylinders. The fibres usually have a deformed morphology, and have been bent, twisted, collapsed, and/or contain holes. Furthermore, the interaction between the papermaking fibres forms multiple sets of chemical bonds and mechanical interlocks that collectively make up the inter-fibre bonds.

The inter-fibre bonds are comprised of breakable hydrogen bonds with a low elastic modulus. These hydrogen bonds are formed between the cellulose within fibrils and the fibre wall, and are generally considered as the major force that holds the structure of paper together [2], along with van der Waals' forces and mechanical interlocks [8, 12]. To a large extent, the strength and number of the inter-fibre bonds as well as the strength of the papermaking fibres control the mechanical strength of a paper handsheet [13]. The properties of paper can be studied at three different levels: paper, network, and fibre [14, 15].

- Paper level: The surface and 2D bulk properties of paper, such as printability, surface roughness, and the quality of the coatings, are related to the density of the paper sheet.
- Network level: The arrangement of papermaking fibres in the network determines the mechanical and optical properties of paper, such as tensile strength, relative bonded area, and opacity.
- Fibre level: The geometry of the fibres has a significant effect on the number of the bonds and the level of the softness of a paper sheet.

The network and fibre level properties are the main factors that can be altered by the production process to increase the quality of the paper. Parameters such as fibre orientation, distribution, and length, as well as tree species can significantly change the mechanical properties of the paper sample. Thus, in order to understand the mechanical behaviour and tensile strength of a paper product, it is necessary to understand and consider the effect of the fibre level and network level properties.

Figure 2.2 – The 3D scanned microstructure of a NBSK based paper sample [16]

2.3 Mechanical Properties

The mechanical properties of paper handsheets are dependent on the geometric characteristics of the fibre network, such as density and thickness. Terminology specific to the pulp and paper industry is used to describe the tensile strength, geometry and morphology of fibres. It is thus necessary to understand these terms before discussing the mechanical properties of paper. The terms and parameters that are used in this thesis are listed below:

- **Papermaking fibre:** Papermaking fibres are small hollow fibres that form each paper/ or pulp sample. These cellulose-based fibres, which are essentially the small tubes in the trunk of the trees, can be easily seen when the edge of a sheet is torn.
- **Lumen:** Lumen is the empty area inside the hollow papermaking fibres. Lumens have a complex morphology since fibres go through multiple compression and drying steps during the paper production process. Recent methods use the lumen to digitalize the microstructure of paper handsheets [15].
- **Lignin:** Lignin is a random, three-dimensional network polymer that holds the structure of wood together. Lignin plays a significant role in binding the fibres together and protecting the trees from the natural degradation. Although lignin is necessary to sustain healthy trees, this compound turns the colour of paper brown, and is generally removed during the papermaking process [17]. The structure of the fibres, lumen and lignin in the wood is shown in Figure 2.3.
- **Inter-fibre bonding:** The microstructure of paper is a random network of fibres that are held together by the inter-fibre bonds. As discussed above, inter-fibre bonds are basically hydrogen bonds that are generated during the drying and pressing steps of the papermaking process [18]. The number of the inter-fibre bonds plays a key role in determining the strength of paper [2].
- **Caliper:** The term caliper refers to the thickness of a paper sheet. It is usually measured in microns (μm).
- **Basis Weight (Grammage):** Basis weight and grammage are comparable terms used in the pulp and paper industry to denote the mass per unit area of a sheet of paper. These parameters are usually expressed in grams per square meters (g/m^2). A normal print paper has a basis weight or grammage of 80 g/m^2 [2]
- **Coarseness:** The coarseness represents the average weight of a fibre per unit length, often reported in units of mg/m. For a given average diameter, it is a measure of wall thickness:

coarse fibres are considered to be less conformable than fine fibres and do not bond as readily [19].

- **Tensile Strength:** The tensile force that is required to produce a rupture in a strip of paper or paperboard, measured in the MD and CD and expressed in kN/m, is known as tensile strength. Tensile strength can be used as a potential indicator of resistance to web breaking during printing or converting. Tensile strength can be calculated using Eq. 2.1 [19], where T is the tensile strength, F is the tensile force and W is the width of the sample.

$$T = \frac{F}{W} \tag{2.1}$$

- **Tensile Index:** The tensile index is a measure of the inherent strength of paper. This parameter is calculated by dividing the tensile strength (T) of a sample to its basis weight and is usually expressed in units of kN.m/kg (Eq. 2.2). Since basis weight has a significant effect on the strength of paper, tensile index can be used to compare the strength of different grades of paper [19].

$$TI = \frac{T}{Basis\ Weight} \tag{2.2}$$

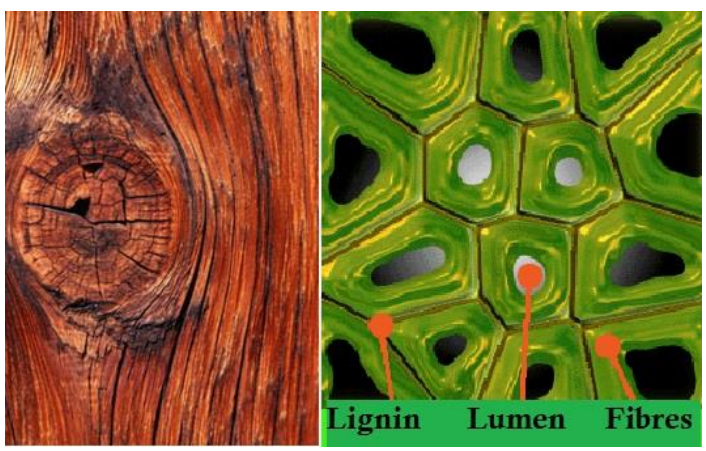

Figure 2.3 – The structure of fibres, lignin, and lumen in the wood [20]

2.4 Experimental tests examining the strength of paper

Various experimental testing methodologies have been utilized to study the mechanical properties of paper and the strength of the papermaking fibres [21, 22, 23, 24, 25, 26]. As early as 1950, it was known that the strength of a sheet of paper is mainly a result of the inter-fibre bonding between fibres. In this early study, it was shown that the load required for tensile failure of a sheet of paper was lower than the load required to fracture an individual papermaking fibre [27]. Further, coloured fibres were used to determine the location of the break in the paper, demonstrating that while weaker fibres break to cause failure, other fibres just pull out of the sheet [28].

Other early experimental tests on the pre-failure behaviour of a new handsheet have shown that the initial response of the sheet under loading is a large strain, which is mostly unrecovered when the load is removed [29, 30]. This initial strain was initially thought to occur because of straightening of the kinks and curls of fibres throughout the paper sheet network. However, another study suggested that the observed permanent strain was due to the breaking of the inter-fibre bonds and redistribution of the stress within the network [31]. Recent studies, such as the work of Seth [32], have shown that the inelastic behaviour of paper is controlled directly by the mechanical properties of the papermaking fibres.

The effect of processing parameters on mechanical properties, in particular the drying stresses and beating process, have been also experimentally studied [24, 25]. For example, it has been shown that the elastic modulus of paper samples that were pressed more during the forming process was greater than normal handsheets [33] due to the corresponding increase in density. Further, it has been shown that the axial stresses that were applied on the fibre during drying had a significant effect on the mechanical properties of the fibres [17].

The mechanical behaviour of paper samples that were generated based on the mixture of different fibre types has been also experimentally examined in multiple reports in the literature [34, 1, 35, 36, 21, 37]. Sampson et al. [37] proposed an experimental test method to determine the effects of basis weight and fibre type on the tensile strength index of low-density paper. In this study, tensile tests were carried out on various paper sheets with basis weights ranging between 2 and 60 g/m^2 for pine and birch based paper samples, and between 5 and 200 g/m^2 for samples formed from spruce fibres. Sampson showed the tensile index and Young's modulus of paper to increase with increasing basis weights up to 60 g/m^2. In this study, the experimental results were compared to Page's constitutive model (reviewed in a later section) [38] showing a good agreement between

the experimentally measured elastic modulus of paper and Page's theoretical predictions. Further, Sampson described that the tensile index of paper depends on two competing effects: strength increasing at low basis weights due to increased efficiency of stress transfer between fibres and decreasing as the probability of weak spots increases at low basis weights [37].

Experimental testing of the mechanical behaviour of paper has been used to calculate the strength of paper handsheets as well as to determine the elements that affect the behaviour of paper products. Experimental results can be used to generate a constitutive model for the mechanical behaviour of paper, however, this method is more cost and time consuming as compared to the numerical simulations. Further, the behaviour of the microstructure of paper cannot be studied with experimental test methods. It has been shown in this literature review that most of the early studies in the pulp and paper field have experimentally tested the bulk mechanical properties of paper. However, it is also necessary to develop a constitutive model to explain the deformation and behaviour of paper in both bulk and network level. Therefore, in the following section, a review of the research studies on modelling the constitutive behaviour of paper and network materials are presented.

2.5 Modelling the constitutive behaviour of paper

In this section, a review of the models that have been used to simulate the constitutive behaviour of fibrous materials is presented, with a focus on the models that were used to study the strength of a paper sheet and/ or a network of papermaking fibres. The models are presented below in two main categories:

1. Bulk models: These models simulate the behaviour of paper at the paper level and as a homogeneous material. The effect of the microstructure of paper is considered in some of these models through the use of a random distribution function.
2. Network models: These models describe the mechanical behaviour of paper at the network level and as a bundle of small fibres, bonds, and voids. In these models, the structure and geometry of the papermaking fibres has a direct relationship on the total strength of the paper sheet.

Network and bulk models approximating the mechanical behaviour of paper have both been developed based on the results of the experimental tests and numerical simulations. Section 2.5.1

and 2.5.2 will review the most-used constitutive models of the mechanical behaviour of paper in the literature.

2.5.1 Bulk constitutive model

One of the first studies on the strength of paper and other fibrous materials was presented by Cox et al. [39]. Cox's tensile strength calculations were based on the concept of an ideal paper, consisting of a perfectly homogenous plane of long straight thin fibres, which are randomly oriented based on a normal distribution function. Within the paper mat, the fibres are assumed to only transfer tensile loads since the flexural stiffness of each fibre is assumed to be zero. For a specified amount of displacement applied to the edge of a sheet, the overall stress is equal to the sum of the local strains on each fibre multiplied by the Young's modulus of each fibre, as shown below,

$$\sigma_x = \int_0^{\pi} E_f\left(\varepsilon_x \cos^2\theta + \varepsilon_y \sin^2\theta + \gamma_{xy}\sin\theta\cos\theta\right)\cos^2\theta\, f(\theta)d\theta \qquad (2.3)$$

$$\sigma_y = \int_0^{\pi} E_f\left(\varepsilon_x \cos^2\theta + \varepsilon_y \sin^2\theta + \gamma_{xy}\sin\theta\cos\theta\right)\sin^2\theta\, f(\theta)d\theta \qquad (2.4)$$

where σ_x and σ_y are the in-plane stresses within a sheet of paper, E_f is the Young's modulus of each fibre, ε_x, ε_y, and γ_{xy} are the global tensile and shear strains, θ is the angle corresponding to the orientation of a fibre with respect to the loading direction, and $f(\theta)$ is the fibre distribution function. The bulk elastic modulus of the paper sheet can then be calculated using Hooke's Law based on the calculated stresses σ_x and σ_y (assuming $\tau_{xy} = 0$), and the applied strains ε_x, ε_y, γ_{xy}. Cox applied the above model to investigate the mechanical properties of a resin-filled planar fibre mat, and showed that for a homogeneous sheet, the elastic modulus was equal to one-third as compared to Young's modulus of an individual fibre. Although this model provided new insight into stress distribution in paper handsheets, the calculated results poorly matched against experimental findings. Cox attributed this differentiation to be caused by the curved morphology of actual papermaking fibres, and the transmission of the load through the inter-fibre bonds. Further, Cox proposed that the stress gradient was dependent on the length of fibres, but due to the differences in the morphology of fibres, no validation was provided for the local strain measurements [39].

The microstructural properties of paper, such as kinks, curls, and the micro-compression on individual fibres were further considered in constitutive models developed by Page and Seth [40],

Lindström et al. [41], and Page et al. [38]. The work of Page is perhaps best-known of these models, and is the most-used. In this model, the bulk Young's modulus (at the level of the sheet) and Tensile Strength are calculated directly, based on the microstructure of the paper, as shown below,

$$E = \frac{1}{3}E_f\left[1 - \left(\frac{w}{L\,RBA}\right)\sqrt{\frac{E_f}{2G_f}}\tanh\left(\frac{L\,RBA}{w}\sqrt{\frac{2G_f}{E_f}}\right)\right] \tag{2.5}$$

$$\frac{1}{T} = \frac{9}{8Z} + \frac{12A\rho g}{bPL(RBA)} \tag{2.6}$$

where in Eq. 2.5, W is the fibre width, L is the fibre length, RBA is the relative bonded area, G_f is the fibre shear modulus, and in Eq. 2.6, T is the tensile strength, Z is the breaking length, A is the average fibre cross section, b is the measured shear bond strength per unit bonded area, and P is the perimeter of the fibre cross section. Page further proposed to include the effect of fibre variations by substituting the length of each fibre with a representative length, ($L_r = \frac{L}{1+n_k}$), where n_k is the number of severe kinks, crimps and curls in the fibre. Note that in Eq. 2.6, the tensile strength of the sheet is expressed in terms of the breaking length [42].

Page applied the above model to a series of different paper types, showing good agreement against experimental data, especially Young's modulus. However, it must be noted that this model is semi-empirical, since n_k and E_f were used to fit the model to the experimental data. Further, it is necessary to experimentally assess RBA directly using optical methods in order to account for the degree of bonding in paper. Page's model has been applied extensively, e.g. [43, 44], where it was shown that while the model is valid many different paper types, the fitting constants are unique to a paper type / paper processing set of conditions.

Bulk models have also been developed to predict the non-linear response of paper to loading in the elastic and plastic regimes. In one study, Xia et al. [45] developed two different isotropic elastic-plastic models for paperboard, and compared against experimental data. The first model was based on a non-quadratic multi-surface yield function, while the second used a non-linear elastic out-of-plane description. The results indicated that such complex nonlinear models can accurately predict the stress-strain response of paper, including the response during folding operations. However, extensive experimental work is required to calibrate the model. In a second study, Makela and Ostlund [46] proposed a model of paper's anisotropic properties based on the

orthotropic elasticity and isotropic plasticity equivalent transformation tensor. This model was used to investigate the mechanical response of a commercial grade copy paper with 60 g/m^2 basis weigh to in-plane tensile loading. The proposed model results were in good agreement with the experimental tensile strength test results. However, the model results were found to be less accurate in describing the out-of-plane behaviour. Further, this model only considered the bulk properties of paper samples and didn't include any geometrical effects of fibres. As shown by Page [38] and Cox [39], fibre geometry has a significant effect on the tensile strength of paper.

Based on the work reviewed above, it can be seen that while the bulk model are suitable for modelling the macro-scale behaviour of paper as a homogeneous sheet, the micromechanical deformations within the fibres as well the bonding stresses cannot be predicted. In order to simulate the corresponding stresses within each fibre and/or the inter-fibre bonds, network models are required. Network models couple the bulk stresses and strains with the geometry of the fibre mat to calculate the local stresses at each fibre. However, clearly, the development of a network model for a fibrous geometry is complex, requiring consideration of the factors that affect the microstructure of paper and papermaking fibres, namely the fibre morphology, bonded area, basis weight, humidity, etc.

2.5.2 Network constitutive modelling

Network models examine the mechanical behaviour of paper based on the knowledge of the microstructure of paper. Due to the significant amount of computational cost that is required for this type of simulations, network modelling of the mechanics of paper was not used in the pulp and paper field as early as the bulk modelling methods, as explained in section 2.5.1. More recent research, such as the work of Heyden [77], has used network approaches. Recently, the generation of artificial fibre networks and realistic meshing of fibre geometry has led to the development and study of micromechanical constitutive behaviour models of paper [47, 48].

A 3D network model was proposed by Lavrykov et al. [48] to study the sheet properties of the network of fibres. The sheet was generated through simulation of the forming and the press sections of the papermaking process. Therefore, fibres were first modelled as jointed beam elements in the forming section and then discretized into simple hollow uniform fibres consisting of a layer of solid elements around the lumen. Inter-fibre bonding was introduced into the model using spring elements. The model was able to estimate the elastic modulus and deformation of the sheet under small strains. In this work, the proposed method was also used to qualitatively study

the effect of fibre geometry and softwood/hardwood fibre mixture on the tensile strength of 60 g/m^2 paper samples. The advantage of this approach was that, because the forming process was simulated, the paper density and RBA were inherent within the simulation geometry. However, since the actual geometry of the fibres was not used for tensile strength simulations (the fibres were assumed to be jointed beam elements), the calculated elastic modulus was much lower than corresponding experimental results found in the literature.

A 2D stochastic computational network model for simulating the uniaxial tensile response of paper was presented by Bronkhorst et al. [49] In this work, a 2D network was stochastically generated by placing papermaking fibres in a 100 mm^2 domain. A FE model of the structure was then created in Abaqus™, modelling the fibres as isotropic elastic-plastic beams with rigid inter-fibre bonding. The stress–strain behaviour generated from simulations was then compared with the tensile strength measurements performed both in the machine (MD) and cross directions (CD). Although the simulation results showed a good agreement with the experimental curves in the elastic mode, the plastic stresses of the simulation were higher than the experimental values.

In comparison to the bulk models, the network models provide a better understanding of the deformation mechanisms of the microstructure of paper. Network models have been used to study both the bulk and network properties of paper sheets. These models utilize a 3D geometry, which enable definition of the fibres, any resulting mechanical interlocks between the fibres, and the inter-fibre bonds.

2.6 Numerical Simulations

While the above literature focused on characterizing the bulk constitutive behaviour of paper (elastic modulus, stress/strain behaviour) through network modelling, in this section, the literature review in this section is focused on study of the microstructural parameters such as the geometry of fibres and basis weight which influence the strength of paper.

2.6.1 Two-Dimensional (2D) simulations

An early FE simulation of the axial behaviour of a network of fibres was presented by Rigdahl, et al. [50]. In this work, the effect of the uniaxial stress on a 2D network of fibres was studied based on the structural element suggested by Perkins [51]. This network model consisted of fibres with a finite length that were oriented in the loading direction and with perpendicular crossing fibres that connected the longitude fibres with rigid inter-fibre bonds as shown in Figure 2.3. Gaps or

holes can be seen in the structure, to approximate the end of one fibre and the start of another. The fibres were modelled using linear-elastic beam elements. Through the simulations, it was shown that strain in a fibre is negligible at the fibre end and reached its peak value where one fibre intersects with another. Moreover, the results indicated that the connected length of fibre is only effective in transmitting load through the network.

simple geometries, such as cylinders and beam elements, have been used in various numerical simulations to reduce the calculation cost [47, 7, 52]. Jangmalm [52] provided a numerical study of the mechanical response of a 2D network of curled cylindrical fibres. The main purpose of this study was to study the effect of the fibre curl, length, and the bonded area of the sample on the elastic modulus of the network. Based on a comparison between the simulation results and the experimental tests performed on commercial pulp, Jangmalm showed that the simple geometry used in the model could not account for the effect of fibre curl see in the experimental results. The authors discussed a number of reasons for this discrepancy, including differences between the 3D nature of paper and the modelled 2D geometry, which removes the effect of the out of plane fibres and bonds.

FE simulations were also used to study the mechanical behaviour of paper samples that were formed based on a random distribution of fibres [53, 54, 55, 56]. Astrom and Niskanen [54] studied the fracture behaviour of a 2D random network of straight fibres using numerical simulation. In this study, uniaxial tensile simulations were performed to study the behaviour of fibres during the fracture process. In each loading step, failed elements were removed from the sample until the complete fracture of the sheet. Astrom and Niskanen indicated that due to the non-uniform distribution of the fibres in the sheet, the fibres were not distorted equally, which resulted in local one-directional fibre fractures. Further, the results showed that the stiffness of the sheet was equal to the stiffness of an individual inter-fibre bond divided by the shear strength of the bond. However, since the model results were not compared against experimental data, the accuracy of the model is questionable.

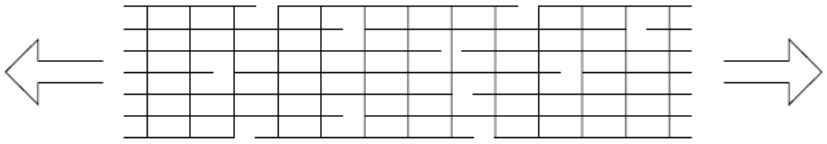

Figure 2.4 – Illustration of the network geometry used for uniaxial tensile strength simulation by Perkins [51]

2.6.2 Three-Dimensional (3D) simulations

3D Numerical simulations have been also used to simulate the mechanical behaviour of paper [57, 48, 47]. A 3D network of paper making fibres, as shown in Figure 2.5, was used to study the effect of the microstructural parameters, such as fibre length and cross section, on the deformation to paper samples at the fibre level [57]. In this study, uniaxial deformation of the paper handsheets were simulated in Abaqus software using various wood fibre types that were meshed with 8-noded brick elements. The contacts between the fibres were generated using the hard contact definition forming an elastic bond with infinite spring constant between the fibres. The uniaxial elastic modulus of each sample was determined from the tensile strength simulations. Based on the results of these simulation, it was shown that the predicted elastic modulus of handsheets with longer fibres were higher than the sheets with shorter fibres.

In another study, Lavrykov et al. [48] performed 3D FE numerical simulations to study the effect of various fibre types on the mechanics of paper at the fibre level. In this study, the elastic strength of paper samples with a constant basis weight of 60 g/m^2 and a range of hardwood/softwood mixtures were calculated using numerical simulation. Although the simulation results provided the elastic modulus of paper handsheets with various fibre types, the simplified geometry of papermaking fibres, lead to much lower values in comparison to the experimental results provided in literature.

The fibre material that is used in the numerical simulation of the strength of paper is often considered to be linearly elastic [25, 58, 59]. Although the elastic material properties can present the deformation of the network of fibres under small strains and loading conditions, the plastic deformation and failure modes of the network cannot be studied. Therefore, numerical simulations have been also used to study the elastic-plastic behaviour of paper (e.g. [60, 49, 61]). Borodulina et al. [61], have investigated the elastic-plastic stress-strain curve of paper using the tensile strength simulation of an artificial network of fibres. In this study, the 3D network of fibres was artificially

generated based on the straight cylindrical fibres that were assumed to have a yield strength of 100 MPa. In these numerical simulations, the effect of the inter-fibre bond was studied based on a breakable elastic bond definition and various bond strength values. Borodulina showed that the influence of the bond strength on the stress-strain curve of the simulated paper was significant. A factor of 2-3 in bond strength changed the strength of the network dramatically. Further, it was shown that due to the local failure of the inter-fibre bonds, a softening happens in the stress-stress curve of paper before the complete failure, which is in a good agreement with the stress-strain curve that was generated based on the experimental results.

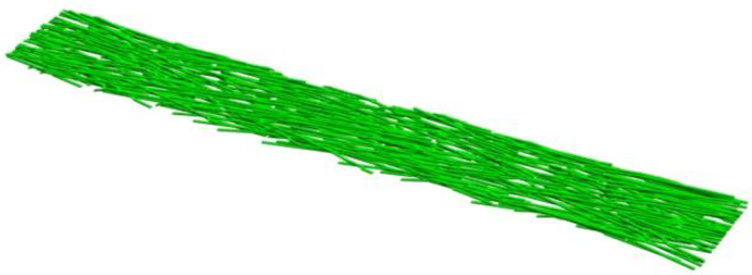

Figure 2.5 – A 3D network of papermaking fibres [57]

Numerical simulation methods, such as FEM, have been extensively used for the numerical simulation of the behaviour of paper. These numerical simulations have been often manipulated using a 2D network of papermaking fibres that were assumed as straight hollow cylinders. Simple Bernoulli beam elements were also used to generate the network samples for the numerical simulations. Since the papermaking fibres have a complex geometry that might have twists, kinks, or holes in the fibre wall, it is necessary to consider their actual geometry in the numerical simulation of the mechanical behaviour of paper. Although a few recent studies have used a 3D network of fibres to simulate the mechanical behaviour of paper, none have considered the actual geometry of papermaking fibres in their simulations.

2.7 Inter-fibre bond strength

The measurement of the strength of an individual inter-fibre bond is not straight forward, both because it requires a careful precision to be formed and to be measured, and also because of the great variation among fibre geometry and bond properties [88]. However, a few studies within the literature have proposed that the bond properties are determined by the strength of inter-fibre

molecular interaction, the number of interaction in the contact area, and the total molecular contact area [18, 62, 12].

The routine methods that have been previously used in the pulp and paper's field to determine the strength of an individual are based on the measurements of either the behaviour of a single fibre bond connecting two fibres, or the effect of the bond on the bulk properties of paper [63, 41]. Measurements at the paper level have the advantage that a large number of bonds are represented in each test, the bond structure is that resulting from the forming process, and the bond is not constructed artificially, and the measurement methods are rational. However, the sheet structure affects the loading behaviour to a great extent and the bond strength cannot be separated from the network strength. Thus the result of a measurement of specific bond strength is valid only for the specific structure and loading mode that is used [12].

A few studies in the literature have utilized high accuracy measuring methods, such as Atomic Force Microscopy (AFM) and Surface Force Apparatus (SFA) to measure the inter-fibre bond strength [64, 65, 66, 67]. In one study, a Surface Force Apparatus (SFA) was used to calculate the energy between the adhesion surfaces of Langmuir Blodgett (LB) cellulose films [64]. Based on these measurements, it was concluded that the interfacial energies of the cellulose surfaces were in the range of 53 and 106 mN/m.

The strength of the inter-fibre bonds was also experimentally and numerically measured under different loading conditions [68, 69, 66, 67]. In the work of Schmied et al. [70], the pre-failure behaviour of an individual inter-fibre bond, connecting two papermaking fibres, was studied under static and dynamic loadings. Specifically, the load was applied to the bond using a calibrated cantilever at the tip of the atomic forced microscopy (AFM) apparatus, which was used to measure the corresponding displacement of the bond. The maximum reaction force of the bond as well as the dissipated energy during the failure was then measured. Figure 2.6, shows the AFM apparatus that was used and the measured force-displacement curve. Schmied showed that although the inter-fibre bond is considered as an elastic spring in most of the literature, the failure behaviour of the bond was dominated by three major factors: breaks in the bundle of the micro-fibrils between the fibres, the breaks of the single micro-fibrils, and delamination of the fibre wall itself. Being one of the only measurements of the strength of the inter-fibre bond in the literature, the results of this study can be used in the numerical simulations that use the network models for simulation of the behaviour of paper.

Magnusson and Ostlund presented a numerical investigation of the strength of an individual inter-fibre bond [71]. In this study, the mechanical behaviour of an individual inter-fibre bond between two artificial fibres was analysed in three modes of loading: peeling, shearing, and tearing, Figure 2.7. The fibres that were used in the bond strength simulations were generated based on the stacking of an idealized fully collapsed cross section over the centerline of an actual papermaking fibre. The semi-realistic morphology of the fibres was discretized using beam elements in for the FE simulations in Abaqus software. The results of the simulation were reported in terms of the 3D resultant forces and moments. Further, Magnusson provided a constitutive elastic model for the individual fibre, which is used in this thesis to model the behaviour of the papermaking fibres. Further details of this approach to modelling of the fibres is discussed in section 4.3.

Hirn and Schennach suggested that Van der Waals forces are the most significant factor in forming the inter-fibre bonds in pulp and paper products [25]. In this study, six mechanisms were suggested for the inter-fibre bonding in paper: inter-diffusion, mechanical interlocking, capillary forces, Coulomb forces, hydrogen bonding and Van der Waals forces. The dissipated energy of the bond was measured for each mechanism and compared to the experimental measurement of the dissipated energy of an inter-fibre bond in cyclic loading and unloading periods. Although energy method is not accurate for comparing the strength of the bond and the effect of the bonds on the strength of the paper sheet, it has been shown that the simulation results of the strength of the inter-fibre bonds that were simulated based on the Van der Waals forces were in the best agreement with the experimental test results.

Based on the work reviewed above, multiple mechanisms are proposed for the nature of the inter-fibre bonds in paper. The mechanisms based on the Hydrogen bonding and Van der Waals forces were considered as the main factors that control the behaviour of the inter-fibre bonds. Although these mechanisms are considered to explain the physics of the bonds, the micro-scale dimensions of the bonded area as well as the complex geometry of network of paper limits the complete mechanical study of the mechanical behaviour of the bond, which leaves our understanding of the molecular mechanisms of bonding in its early stages [41].

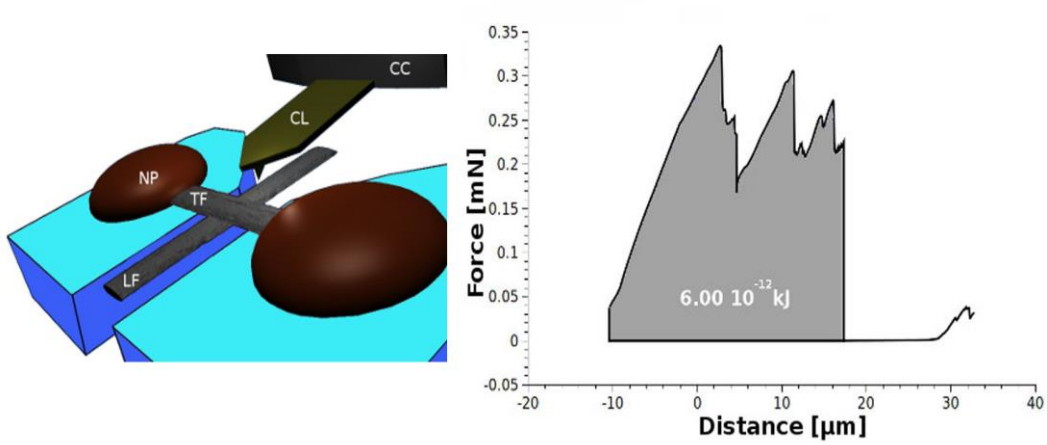

Figure 2.6 – The bond testing apparatus and the calculated deformation - force curve of the peeling test, presented by Schmied et al. [70]

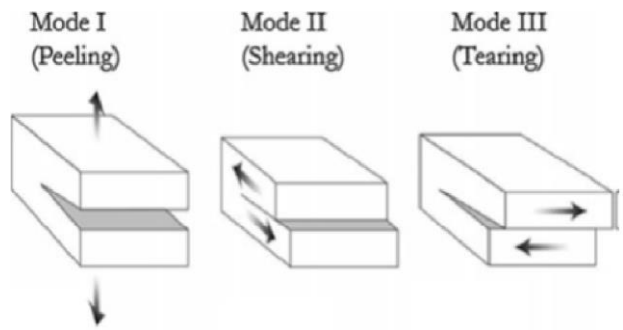

Figure 2.7 – Modes of loading in tensile strength analysis of an inter-fibre bonding [71]

2.8 Imaging methods

The constitutive behaviour of paper has been numerically studied in recent years based on the actual geometry of the fibre network at the microstructural level. Meshing the actual geometry was made possible by scanning the morphology of papermaking fibres using high resolution imaging techniques such as Scanning Electron Microscopy (SEM), Atomic Force Microscopy (AFM), and X-ray micro tomography (µCT) [14]. SEM has been used extensively in the literature to study the surface properties of paper, for example, for measuring the local micro roughness of paper based on stereo images (Reme and Kure [72]). Although the SEM images provide high-resolution information about the surface of the scanned sample, they are not able to provide significant information about the 3D structure of paper. AFM provides higher resolution images compared to SEM, which enabling the study of the interaction of fibres [15]. The applicability of AFM for performing surface measurements on paper handsheets was demonstrated by Hanley [73]. The

AFM method was also used by Schmied et al. [70] to measure the generated gap between the bonded papermaking fibres in a peeling test. Although the above imaging techniques provide high-resolution images of paper, none can be used to generate a 3D mesh for the numerical simulations. An alternative technique, X-ray Micro Computed Tomography (μCT) is a novel and non-invasive method for acquiring high-resolution images from the 3D structure of various materials. The applicability of this method for 3D visualization of the microstructure of paper was demonstrated by Sharma et al. [16], amongst others. In this study, a high-resolution structure of paper was visualized in 3D using X-ray μCT. This 3D structure can be used as a base mesh for the FE simulations of the mechanical behaviour of paper.

2.9 Summary

The experimental tests and numerical simulations that have been used in the past to study the mechanical behaviour of paper have been reviewed in this chapter. Using the experimental tests, bulk properties of sheet, such as Young's modulus and tensile index, have been calculated. However, the mechanical behaviour of the paper at the fibre level cannot be studied using the experimental testing methods alone. Numerical schemes such as FEA provide a mechanism to study the mechanical behaviour of the microstructure of paper as well as the effect of the morphology of fibres on the bulk properties of the sheet. Most of the prior work has utilized a 2D samples for the simulations with fibres that were assumed as idealized shapes, such as hollow cylinders and beams. Since the complex morphology of the papermaking fibres have a direct effect of the strength of the paper sheet, it is necessary to consider their actual geometry in the numerical simulations. Although recent numerical simulations have often used the 3D network of papermaking fibres or softwood/hardwood mixtures, none have considered the actual geometry of papermaking fibres in their simulations. The strength of an individual inter-fibre bond has been also studied both experimentally and numerically. These studies have investigated the behaviour of the bond in various loading conditions, which can be used to model the bonds in the numerical simulation of the tensile strength of the network of papermaking fibres.

Chapter 3: Scope and Objectives

Deformation of the microstructure of paper and the interaction of papermaking fibres can be studied by both experimental methods and numerical simulations. It was shown in chapter two that the previous efforts for numerical modelling of the mechanical behaviour of paper has been successful to estimate the bulk strength of paper; however, these simulations couldn't demonstrate the effect of some of the micro-scale parameters, such as: inter-fibre bond strength, actual morphology, and the network orientation of fibres. Therefore, recent studies in the field of the mechanics of paper are more focused on the understanding of the physics at the micro-scale as well as finding the major elements that affect the strength of paper. These efforts can be categorized in two main groups: the study of the behaviour of an individual inter-fibre bonds and investigation of the effect of the actual morphology of fibres on the strength of the paper sheet. One method that has been recently used to obtain the actual fibre geometry is X-ray Micro Computed Tomography (μCT).

FE simulations of paper that utilize the actual geometry of papermaking fibres can provide a realistic estimation of the mechanical behaviour of the complex microstructure of paper. Based on the high-resolution visualized geometry of NBSK pulp fibres, the strength of paper samples with a softwood/hardwood mixture can be numerically simulated. Having these benefits in mind, the objective of this thesis is to develop a numerical simulation to study the tensile deformation in low density hardwood/softwood mixtures using the actual meshed geometry of NBSK fibres generated from 3D micro-tomography of paper handsheets.

In order to achieve this objective, the following methodology is used:

1. Generation of a 3D mesh of the actual papermaking fibres based on the scanned μCT images.
2. Simulation of the mechanical behaviour of an individual inter-fibre bond.
3. Generation of 3D networks of papermaking fibres based on the 3D meshed geometry of the fibres.
4. Simulation of the uniaxial deformation of low density paper handsheets.
5. Validation of the simulation results in comparison with the results of the experimental tensile strength tests of the paper handsheets.

The details of the outlined methodology for both groups of the simulations are described in chapter 4, “Finite Element Simulations”, including the geometry (based on scanned CT images), mesh, and boundary conditions, as well as simulation parameters such as the time increments. Since mesh size is the main element that changes the calculation time and the amount of the memory needed for the simulation, specific protocols are followed for mesh generation to minimize the calculations while maintaining the actual morphology of fibres in the meshing. Two groups of numerical simulations are then developed based on the meshed geometry: simulation of the peeling strength of an individual inter-fibre bond, and simulation of the mechanical behaviour of the network of fibres under uniaxial tensile loading. In the bond strength simulations, the characteristics of the bonding definition between the fibres were determined based on a previously published experimental work on the mechanical behaviour of the inter-fibre bond [70]. Therefore, the boundary conditions that were applied to the fibres in these simulations were set to mimic the behaviour of the fibres in the experimental set-up. Each group of the simulations were repeated with various types of fibres to study the effect of fibre morphology on the behaviour of the inter-fibre bonding as well as the network of fibres. Furthermore, the tensile index of the network of fibres as well as the required force and dissipated energy to break an individual inter-fibre bond is calculated. The results of the simulations are then presented and discussed in chapter 5, “Results and Discussions”, which is followed by final conclusions in chapter 6, “Conclusions”.

Chapter 4: Finite Element Simulations

4.1 Overview

This chapter presents the details of the methodology that was used for the Finite Element (FE) simulations on paper. As stated in Chapter 3, two groups of simulations were conducted to study the mechanics of paper:

1. Simulations representing the mechanical response of an individual inter-fibre bond to a peeling load.
2. Simulations representing the tensile strength of low density paper.

These simulations were conducted to study both the behaviour of the individual inter-fibre bond and the bulk properties of paper. For the first time, the true geometry of papermaking fibres was used for numerical simulations of papermaking fibres. This geometry was obtained from a 3D X-ray tomographic microscopy image of a paper handsheet. This chapter explains the sample preparation, meshing of the actual papermaking fibres, material properties, boundary conditions, and approach used to model the inter-fibre bond.

In Section 4.2, the methodology for creating the simulation geometry is explained including μCT scanning to acquire 3D images of real paper handsheets, subsequent image processing to segment individual fibres, and meshing. In Section 4.3, the methodology for simulating the strength of a single inter-fibre bond is explained. Section 4.4 presents the methodology for simulating the bulk properties of low density paper samples based on NBSK fibres. This section also explains a novel artificial fibre generation code that was written to form the fibre network of the simulation geometry. Since the actual geometry of NBSK fibres is used in both simulations, the geometry of the placement of these fibres has a major effect on the simulation results. Control over fibre placement provides new insight into the relationship between the micro-scale properties of papermaking fibres, i.e. length and fibre type, and the macro-scale tensile strength property.

4.2 Generation of the Simulation Geometry

The actual shape and structure of NBSK fibres were used to create the geometry for both groups of FE simulations, in order to provide an accurate analysis on the effect of fibre morphology on the mechanics of the inter-fibre bond and paper. First, a paper handsheet was scanned using X-ray tomographic microscopy. Then, individual fibres were segmented from the 3D dataset and meshed.

4.2.1 Imaging and Segmentation of the Fibres [15]

A µCT apparatus (Zeiss Micro XCT-400 X-ray tomographic microscopy) located at UBC Okanagan's campus was used to scan a paper handsheet consisting of 100% NBSK fibres and fabricated at UBC's Pulp and Paper Centre (PPC). A dataset 1.0 x 1.0 mm^2 in cross-section and 250 microns in thickness was acquired at a voxel size of 0.53 µm. This volume contained 1500 fibres, as shown in Figure 4.1. The segmented fibres were then labeled based on their corresponding greyscale value, separating the high density fibrous content of the images from the void spaces between the fibres. The labeling process enabled extraction of individual fibres from the geometry. The geometry of the labeled fibres is shown in Figure 4.2.

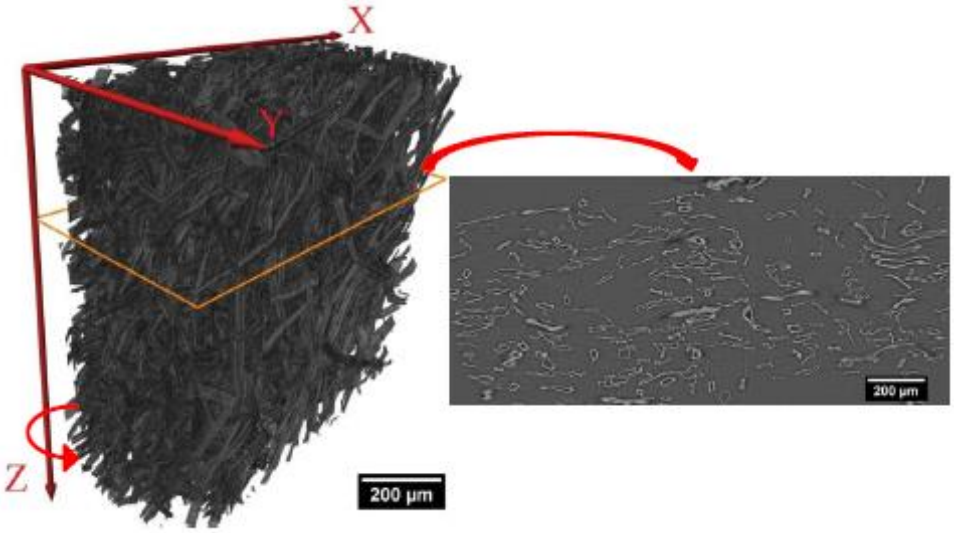

Figure 4.1 – 3D visualization of the microstructure of paper [16]

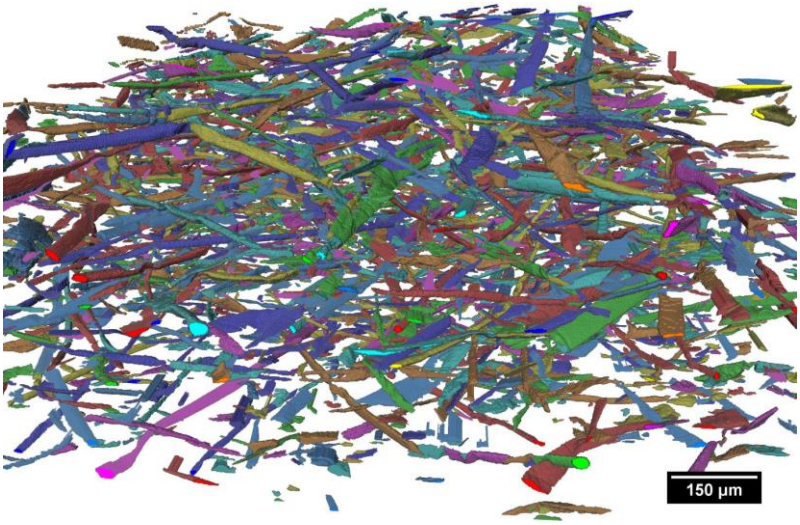

Figure 4.2 – The network of labeled papermaking fibres [16]

4.2.2 Fibre Extraction

While the 3D geometry of paper that was generated from the scan of paper handsheets provided extensive information about the microstructure of paper and papermaking fibres, this geometry cannot be directly used in the FE simulations because of the large size of the dataset, and the large number of small unconnected regions (small paper fragments) that are present. Therefore, the individual fibres were extracted from the geometry to artificially form the network.

In order to accomplish this task, a MATLAB script was written to separate individual fibres from the original dataset. Using this code, each fibre was selected based on its greyscale value and isolated from the main geometry. All of the other voxels in this sub-volume were considered voids. An example of two fibres that were separated from the whole geometry is shown in Figure 4.3.

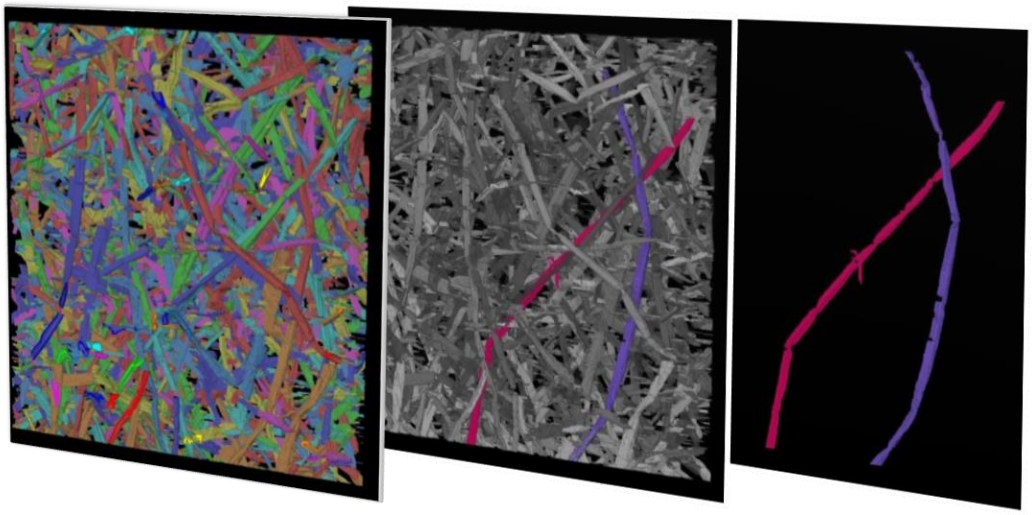

Figure 4.3 – Selection of two papermaking fibres based on their greyscale value

4.2.3 Mesh generation

Each individual fibre extracted from the dataset was then mesh using the +FE Free meshing tool within the ScanIP software. This software uses a tetrahedral meshing algorithm to create the volumetric mesh. The +FE Free meshing algorithm provides great flexibility to replicate the actual morphology of fibres: kinks, twists, and/or holes. The +FE Free meshing tool was used in basic mode to create the mesh for the first group of simulations (peeling simulation of the individual inter-fibre bond). Specifically, the compound coarseness slider, which has a range of-50 to +50, (coarse to fine), was set to -50. Although this created a coarse mesh, the geometrical characteristics of the fibres were closely reproduced by the mesh, as shown in Figure 4.4.

Figure 4.4 – Illustration of the scanned and meshed geometry of a papermaking fibre

Although the basic parameters within ScanIP provide a simple way to mesh the fibres, the result is a relatively high mesh density. For the second group of simulations (tensile strength simulations), the advanced parameters within the software were utilized. This was needed to reduce computational cost. The meshing parameters, listed in Table 4.1, were chosen to compromise between mesh size and quality.

Table 4.1 – Advanced meshing parameters

Compound Coarseness	-40
Target minimum edge length (µm)	3.3
Maximum edge length (µm)	8.2
Target minimum error (µm)	0.1
Surface change rate	80
Internal change rate	30

In this table, the *target minimum edge length* and *maximum edge length* correspond to the smallest and largest edge lengths that will be used in the algorithm to generate the elements, the *target minimum error* is the distance error that the re-meshed surface is allowed to have as compared to the original structured mesh, the *surface change rate* determines how fast the element size can increase on a surface, higher values reduce the element density and lower values increase the mesh adaptation to the actual morphology of the object, and the *internal change rate* determines the mesh density inside of the object; higher values dramatically reduce the number of elements and hence the simulation time as well.

The properties of the mesh that was generated based on the tomography fibres are shown in Table 4.2. In this table, the number of the tetrahedral elements, the triangles of the surface mesh, and the dimensions of the surface and edge of the tetrahedral elements of each fibre are presented. As explained in section 4.2.3, the fibres were meshed using tetrahedral elements in ScanIP software. Therefore, the surface of the fibre was meshed with triangular elements first and then tetrahedral elements were generated from the triangles to form the volume mesh of the fibre. The meshed geometry of the fibre is shown in Figure 4.5.

Table 4.2 – The size and number of the elements of the meshed tomography fibres

	Set 1	Set 2	Set 3	Set 4	Set 5	Set 6	Set 7
Number of elements	94134	38037	48928	78849	70167	74621	56677
Number of triangles	45637	17393	25039	38160	35358	37501	24882
Mean element edge length (µm)	2.64	2.81	3.38	3.26	2.53	3.06	3.06
Mean triangle area (µm^2)	3.83	3.38	5.05	4.73	3.72	4.1	4.1

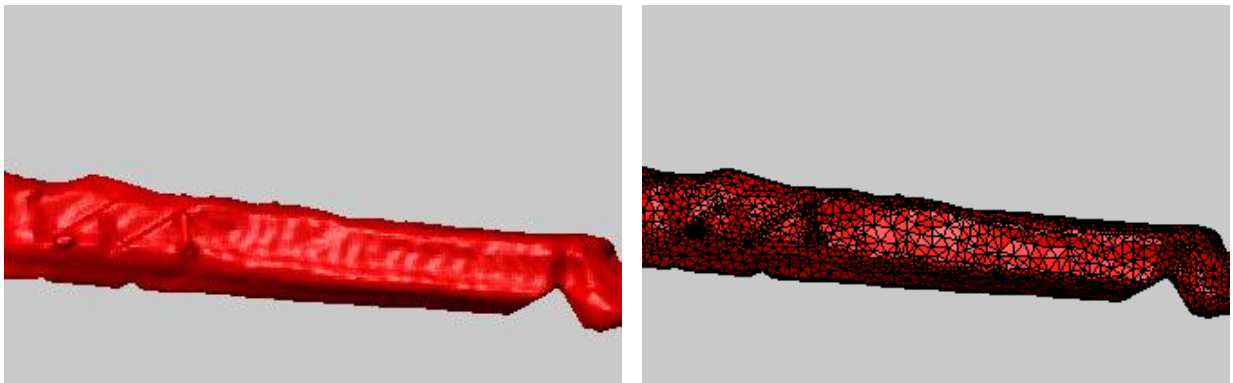

Figure 4.5 – The actual scanned geometry of a papermaking fibre (Left), 3D mesh of a papermaking fibre (Right)

4.2.4 Assembly of the geometry

In this section, the meshing algorithm, extraction of fibres and µCT scans that were used in this thesis have been explained. Individual fibres were extracted from the whole geometry for the FE simulations of the mechanics of paper. Although the meshing parameters were set to match the actual morphology of the fibres, the coarsest mesh in ScanIP was considered in the meshing algorithm to reduce the simulation time. These fibres were then used to simulate the peeling strength of an inter-fibre bond, section 4.3, and the bulk mechanical properties of low density paper, section 4.4. The final stage is to assemble individual fibres into a collection of fibres for mechanical simulation. The methodology for fibre assembly is detailed within the methodology sections for each of the two modelling approaches – simulation of the behaviour of the inter-fibre bond as well as simulation of a handsheet.

4.3 Simulating the behaviour of the inter-fibre bond

Numerical simulations were performed to study the peeling strength of the inter-fibre bond based on the actual geometry of papermaking fibres. In these simulations, inter-fibre bonds were defined between seven pairs of similar papermaking fibres. In each simulation one fibre was fixed at top and the second was placed at 90 degrees and bonded to the top fibre. A displacement boundary condition was then applied to the lower fibre at the closest element near the inter-fibre bond to simulate the elastic deformation of the bond. The pre-failure behaviour of the bond was simulated with a linear elastic spring. The bond was stretched until failure occurred at a defined stress value, and evolved based on a linear energy criterion. These simulation results were then used to calculate the reaction force and dissipated energy of the bond. Figure 4.6 shows the geometry that was used for one of the simulations. The geometry of the fibres, boundary conditions, bond formations, and the material properties that were used in the simulations are explained in the following sections.

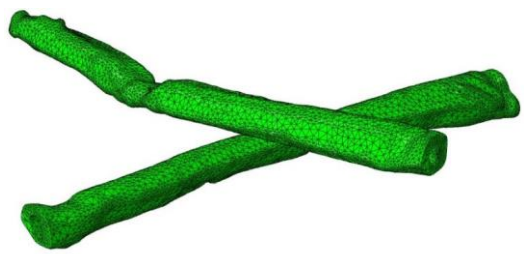

Figure 4.6 – 3D orientation of fibre in the network

4.3.1 Geometry

Seven fibres were extracted from the tomography dataset for the bond-strength simulations. The fibres were chosen based on their length and morphology to represent a wide range of fibre lengths and diameters. In each simulation, one of the fibres were used to create a bonded fibre pair, i.e. the same fibre was used as the top and bottom fibre, resulting in 7 pairs of fibres with various morphologies. The dimensions of the extracted fibres are listed in Table 4.3, where the properties of the fibres were measured as described below:

- Length (L): The length of the fibre was calculated along the centre-line of the fibre through the sequence of the images of the μCT scans. In this process, the location of the centre point of the cross section of the fibre in each image was calculated and a straight line was then drawn from this point to the centre of the cross section of the fibre in the next slice. The summation of the

length of these connection lines between the slices along the fibre length was assumed as the actual length of the fibre.

- Equal Diameter (D): The average equal diameter of the fibre was calculated based on the cross section of the fibre in the images of the μCT scans. In each image, the location of the centre point of the cross section was calculated and the distance between the furthest point on the fibre wall from the centre point was assumed as the fibre radius. The diameter of the fibre was then calculated based on the measured radius. An average of the calculated diameters was considered as the equal diameter of the fibre.
- Fibre Wall Thickness: Similar to the fibre's diameter, the average number of the voxels between the fibre lumen and the surface in the thickness direction were used to calculate the fibre wall thickness.

The length of the corresponding fibres ranges from 440 to 1500 μm, and the equal diameter of the fibres is between 27 to 45 μm, providing a wide range of fibre morphology, which can provide new insight into the effect of fibre morphology on inter-fibre bond strength.

Table 4.3 – Dimensions of the selected fibres for the individual inter-fibre bond strength simulations

	Set 1	Set 2	Set 3	Set 4	Set 5	Set 6	Set 7
Length (μm)	1500	440	663	930	863	995	680
Equal Diameter (μm)	45	33	50	55	35	27	30
Fibre Wall Thickness (μm)	5.5	7	6.5	8.5	5.5	7	12.5

4.3.2 Material properties

The material properties of each fibre were defined in the local coordinate system of the fibre and based on material property values that were previous published by Magnusson and Ostlund [71]. As presented in Table 4.4, the material properties of each fibre were defined using a transversely-isotropic elastic modulus, meaning that the elastic moduli of the fibre along with the fibre's axis direction is different from the isotropic elastic modulus in the cross-section plane. The corresponding material properties were applied to each fibre in its own local coordinate system, which causes anisotropic elastic properties of the sample. A schematic of the local coordinate system of a fibre is given in Figure 4.7.

Table 4.4 – Elastic material properties of the fibres

E_1 (GPa)	E_2	E_3	ν_{12}	ν_{13}	ν_{23}	G_{12}	G_{13}	G_{23}
11.76	1.07	1.07	0.022	0.022	0.39	0.5	0.5	0.38

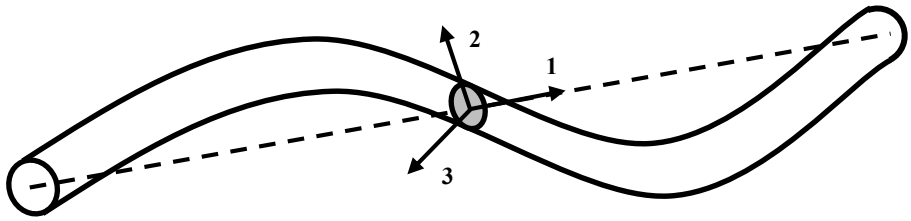

Figure 4.7 - Local coordinates of a papermaking fibre

4.3.3 Inter-fibre bond

The inter-fibre bond between the fibres was defined based on a cohesive behaviour option within Abaqus, and the work of Schmied et al. [70]. As explained in section 2.7, in Schmied et al. the pre-failure behaviour of an individual inter-fibre bond connecting two papermaking fibres was studied under static and dynamic loadings using atomic force microscopy. In this previous work, the reaction force and dissipated energy of the bond during the pre-failure loading were measured, as shown in Figure 4.8.

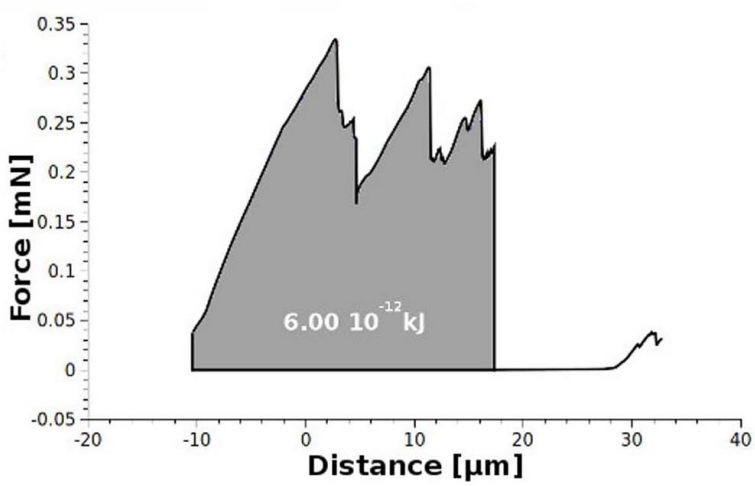

Figure 4.8 –The force-displacement curve of the peeling test, presented by Schmied et al. [70]

In the present thesis, the inter-fibre bonds between the fibres in the peeling simulations were defined based on the Schmied's force-displacement results. In order to model the bonds between the fibres, a breakable surface-based cohesive definition in Abaqus was used that assumes the bond as a spring with an initially linear elastic behavior followed by the initiation and evolution of damage. As it can be seen in Equation 4.1, the elastic behavior is assumed as a diagonal elastic constitutive matrix that relates the normal and shear stresses of the bond to the normal and shear separations between the fibres,

$$\begin{Bmatrix} \sigma_n \\ \sigma_{t1} \\ \sigma_{t2} \end{Bmatrix} = \begin{Bmatrix} K_{nn} & 0 & 0 \\ 0 & K_{t1} & 0 \\ 0 & 0 & K_{t2} \end{Bmatrix} \begin{Bmatrix} \delta_n \\ \delta_{t1} \\ \delta_{t2} \end{Bmatrix} \tag{4.1}$$

where σ_n, σ_{t1}, σ_{t1} are the normal and tangent stresses (in 2 directions) of the bond, K_{nn}, K_{t1}, K_{t2} are the elastic modulus of the spring in normal and tangent directions, and $\delta_n, \delta_{t1}, \delta_{t2}$ are the separation distance between the fibres. Further, it was assumed that the bond is elastic until damage initiates once a certain normal stress (S_{max}) is reached. Damage is then assumed to evolve based on a linear energy criterion. The bond is then completely broken once a final separation point (d_{max}) is reached, as shown in Figure 4.9.

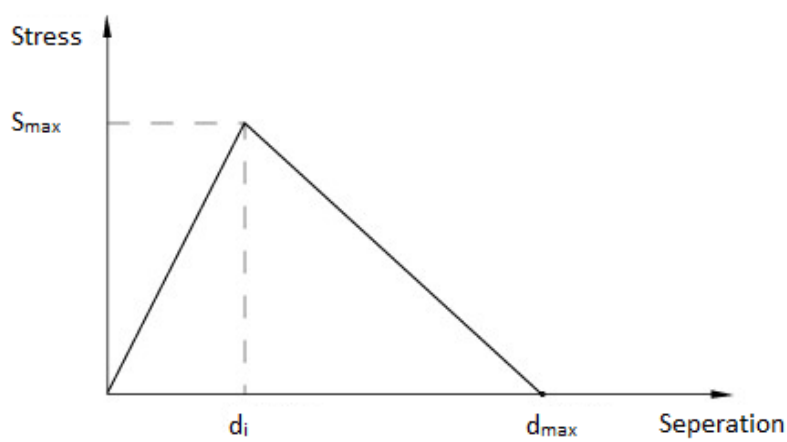

Figure 4.9 – The behaviour of the cohesive bond

While the cohesive-element bonding behaviour with damage criterion within Abaqus requires three input parameters: Spring Constant, Cohesive Bond Strength, and Damage Evolution, Schmied's experimental results were presented in terms of the reaction forces and desperation of the bond. To determine these input parameters, a regression analysis was performed, comparing the required reaction force as a function of relative separation predicted by the simulations against the Schmied's measurements. As can be seen in Figure 4.10, a damage evolution criterion of 3×10-

3 N.µm led to a dissipated energy of 6×10-12 kJ, which was in a good agreement with the experimental measurements. The other parameters were similarly determined (spring constants: 3×10-4 N/µm, cohesive bond strength: 1.7×10-4 N/µm3). Figure 4.11 shows the peak force and area under the force-displacement curve that were used for the definition of the cohesive behaviour.

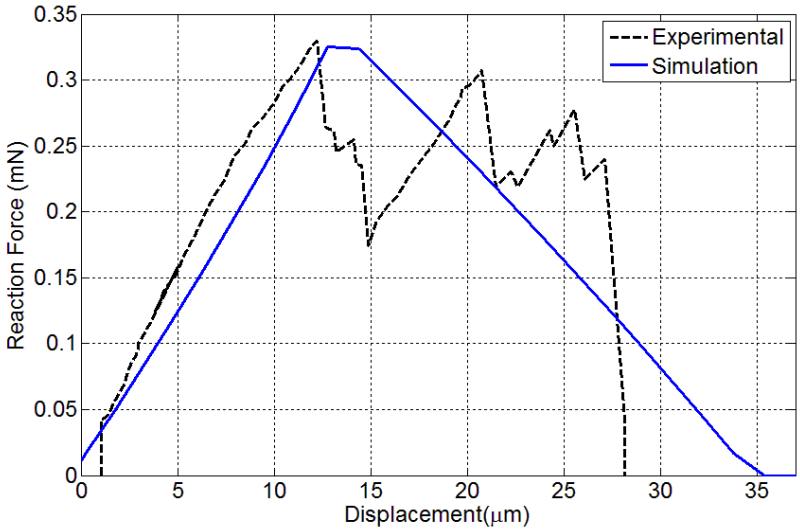

Figure 4.10 – The behaviour of the simulated inter-fibre vs experimental results

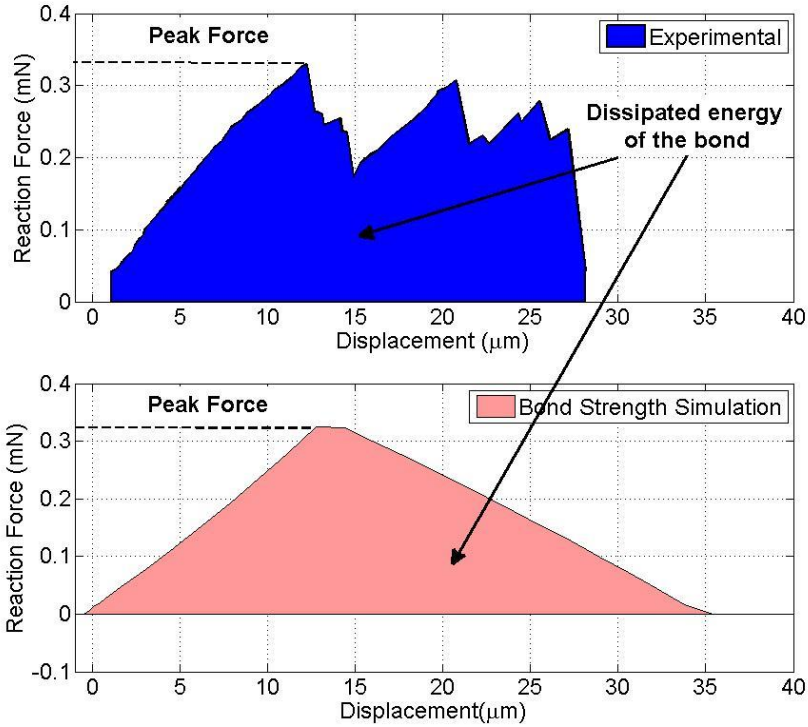

Figure 4.11 – Dissipated energy and fracture force of the experiments (top) and simulations (bottom)

4.3.4 Boundary conditions

In order to mimic the peeling behaviour of the inter-fibre bond, the following boundary conditions were applied to the fibres (also illustrated in Figure 4.10):

- A fixed boundary condition was applied to the nodes at the ends of each top fibre, sides of the top fibre, avoiding any displacement or rotation. ($U_{x,y,z} = 0$, $R_{x,y,z} = 0$)
- A vertical displacement was applied to the bottom fibres at the nearest element to the bonded area (U_z).

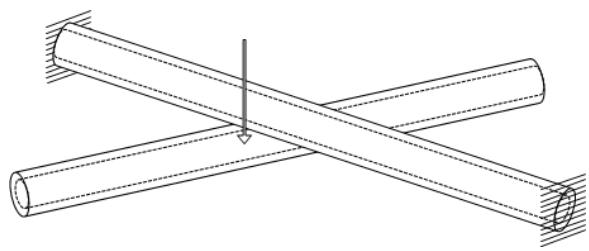

Figure 4.12 – Boundary conditions of the simulation of the individual inter-fibre bond

4.4 Simulation of the strength of the network of fibres

In this section, the methodology that was used to simulate the mechanical behaviour of low density paper is explained. Tensile strength simulations were performed in Abaqus based on the actual geometry of the NBSK fibres. An artificial fibre generation code that was written in MATLAB was used to create the simulation geometry along with the meshed real fibres as explained in section 4.2.

The numerical strength analysis of the fibre network involved multiple sequential simulations. First, the artificial fibre generation code was run to create the simulation geometry. Second, the simulated fibre network was compressed in the thickness direction. Third, the sheet was deformed under a uniaxial tensile displacement. In the following sections, each of these steps is explained.

4.4.1 Generating the Artificial Network of Fibres

4.4.1.1 Artificial Fibre Generation Code

An automatic random positioning algorithm was written in MATLAB to place the meshed fibres within a 3D domain. In this script, the size of the volume, the length, the diameter, and the desired number of fibres in the network were set as the inputs of the code. The fibres were sequentially placed in the network in random positions with random orientations. Note that, for this script, the fibres were assumed to be cylinders, and not the complex shape seen in the tomographic images

and meshed as outlined in section 4.2. The 3D orientation of each fibre was defined using two angles: the first angle (θ_1) was defined around the thickness direction (Z-axis), which ranged between -180° and 180°, and changes the planer orientation of the fibre. The second angle (θ_2) was defined between the centre line of the fibre and the in-plane direction of the network (X-Y plane). θ_2 was defined to range only between -15° and 15°. This resulted in a generated network that was realistic as compared to the X-ray tomographic image of the paper handsheet. A schematic of the two controllable angles is shown in Figure 4.13. A comparison between the actual 3D view of the paper handsheet and the artificially generated fibres is shown in Figure 4.14.

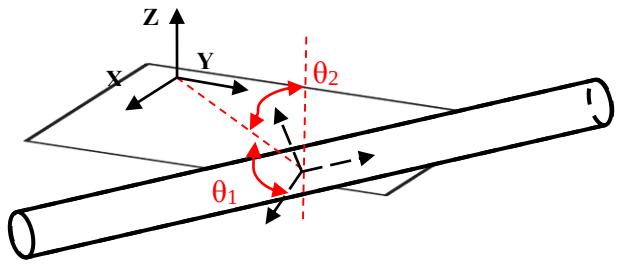

Figure 4.13 – the angles that were used for the 3D orientation of a fibre in the artificial fibre generation code

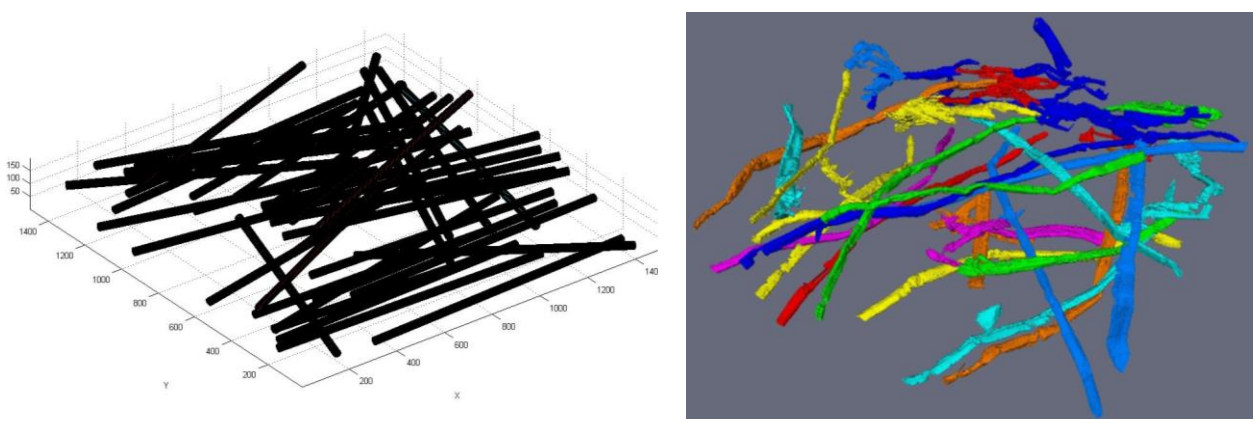

Figure 4.14 – The artificial network of fibres (left) and the network of actual papermaking fibres (right)

In order to prevent the overlapping between fibres, two intersection checks were performed after placing each fibre in the network:

Overlap check: Each fibre was checked to determine if it intersected with other fibres that were previously placed in the network. A specific part of the volume was addressed to each fibre and if this volume was occupied by the other fibres, the new fibre was marked with the intersection error, therefore, the algorithm would generate a new random position (and orientation) to place the fibre. This continued until an intersection-free location was found.

Boundary check: The position of each fibre was also checked against the boundaries of the defined volume. If this requirement was not met, the algorithm would generate a new random position (and orientation) to place the fibre inside. This process was repeated until an appropriate location was determined.

Due to the overlapping criterions, various locations and orientations was tested to place the fibre inside the volume without intersection with other fibres. The number of these iterations will dramatically increase with increasing basis weight, i.e. fibre density. The full algorithm for the artificial fibre generation code is described in Figure 4.15.

The orientations and locations of the artificial fibre generation script were then used to place the actual geometry of the NBSK fibres in the tensile strength simulation geometries. However, due to the differences between the morphology of the cylinders of the script and the NBSK fibres, the generated simulation geometries had overlapping regions between the fibres. Therefore, the simulation geometries were checked for overlaps. In case of the overlapping area between a pair of fibres, the corresponding top fibre were moved in the thickness direction to separate the fibres.

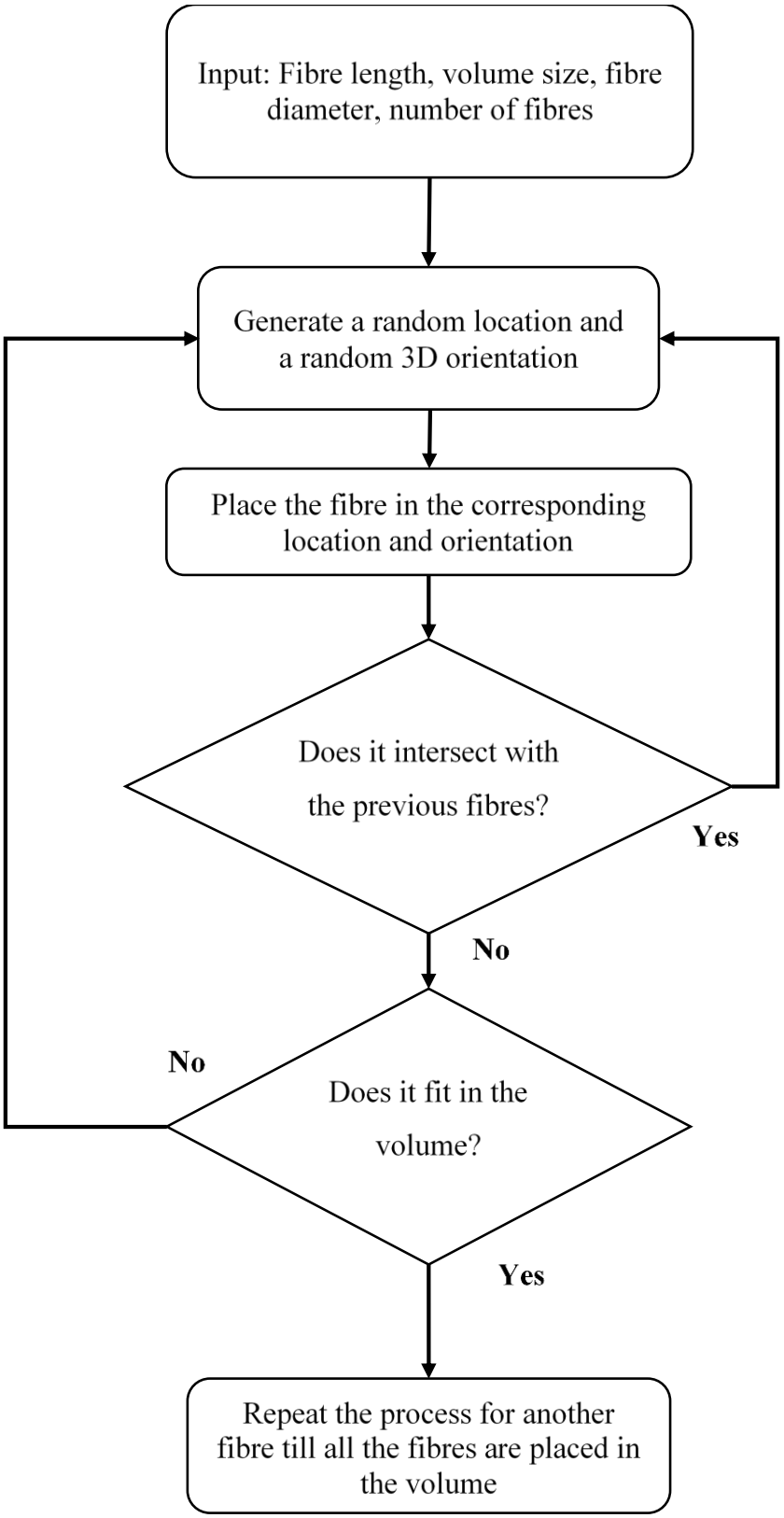

Figure 4.15 – Algorithm of the artificial fibre generation code

4.4.1.2 Incorporating the µCT scanned and meshed fibres

Low-density paper samples were generated for the FE simulations by stacking the meshed papermaking fibres in random positions within a predefined network. The random positions of the fibres were generated by the MATLAB script explained in section 4.4.1. Two fibres, with different lengths, were selected from the µCT images of the scanned microstructure of paper handsheets to provide various morphological properties in the FE simulations: a fibre with a relatively longer length that represents softwood, and a shorter fibre that represents hardwood. The meshed morphology of these fibres is shown in Figure 4.16.

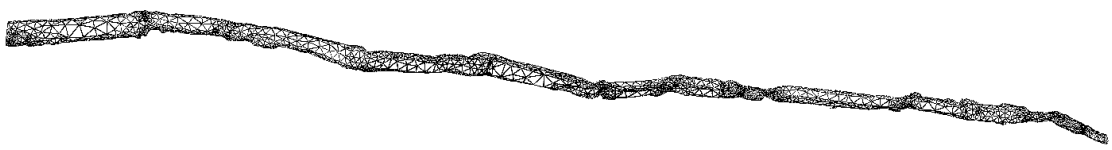

(a)

(b)

Figure 4.16 – Scanned geometry of (a) a softwood Fibre and (b) a hardwood Fibre

The dimensions and physical characteristics of these two fibres are also presented in Table 4.5, where *tortuosity* is defined as the length of a straight line connecting two ends of the fibre divided by the actual length of the fibre, and *equal diameter* represents the average value of the maximum distance between the centre of the fibre's cross section and the fibre wall at each fibre's cross section. The fibre was assumed to have the density of cellulose, 1500 Kg/m^3.

Table 4.5 – Morphological characteristic of the meshed fibres

	Long Fibre	Short Fibre
Length (µm)	2424	1363
End-to-end Length (µm)	2028	1126
Tortuosity	1.195	1.21
Equal Diameter (µm)	22	20
Volume (m^3)	1.13 E-12	5.58 E-13
Mass (gr)	1.70 E-06	8.37 E-07

Using the selected fibres and the MATLAB script, low basis weight network geometries were generated. Each simulation geometry was formed by replacing the cylindrical fibres generated by the MATLAB script by the scanned fibres. In order to study the effect of the morphology of fibres, and mixture rules on the mechanical strength of low density paper, the simulation geometry was formed with various meshed fibres, representing both softwood and hardwood fibres. The characteristics of the different simulation geometries that were used in the tensile strength simulations are listed in Table 4.6:

Table 4.6 – List of the simulation geometries for the Tensile Strength Simulations

	Mono-fibrous Simulations				Softwood/Hardwood mixtures (mass percentage of hardwood fibres)					Simulations with various Young's Moduli		
	Softwood Fibres		Hardwood Fibres		0%	14%	33%	60%	100%	4.5 GPa	11 GPa	23 GPa
Number of fibres	10	20	20	40	20	20	20	20	20	20		
Basis Weight (g/m2)	9.2	18.4	9.1	18.2	18.4	16.1	13.7	11.4	9.1	18.4		

For comparison purposes, additional simulations were carried out on simple hollow cylinders. This allowed for investigation of the effect of the actual geometry of the NBSK fibres on the strength of the sheet. These cylindrical fibres were used to form two geometries with basis weights equal to the group 1 samples (9.1 and 18.2 g/m2). The relevant dimensions are listed in Table 4.7.

Table 4.7 – Morphological characteristic of the cylindrical fibre

Length (μm)	2424
Tortuosity	1
Equal Diameter (μm)	40
Volume (m^3)	1.33E-12
Mass (gr)	2.00E-06

4.4.2 Simulation Steps

The deformation of the paper samples was simulated in two steps:

1. Compression Step
2. Tensile Deformation Step

In the first step, each sample was compressed between two rigid planes to decrease the thickness of the sample and also help the contacts to be formed between the fibres. In the second step, uniaxial tensile elastic deformation was simulated. In the following section, each simulation step is described including the boundary conditions, material properties, and simulation time steps.

4.4.2.1 Compression simulations

The compression simulations were performed in Abaqus by compressing the simulated handsheet between two rigid planes. An example of the geometry that was used for these simulations is shown in Figure 4.17. The compression simulations were used to remove the gaps in the generated network of fibres that were created by the Artificial Fibre Generation code.

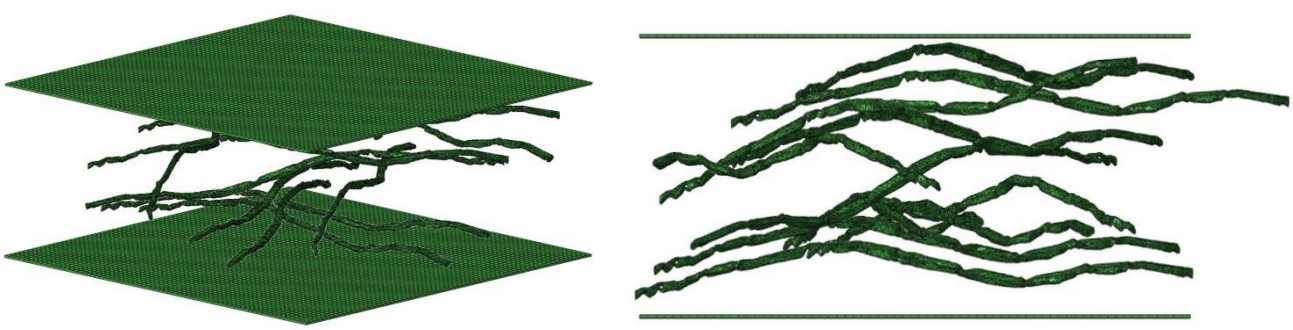

(a) **(b)**

Figure 4.17 – The geometry of the compression simulations, a) isometric view, b) front view

4.4.2.1.1 Boundary Conditions

In order to perform the desired compression behaviour in the simulations, the following boundary conditions were applied to each geometry:

- A fixed boundary condition was applied to the nodes of the bottom plate, avoiding any displacement or rotation. ($U_{x,y,z} = 0$, $R_{x,y,z} = 0$)
- A vertical displacement was applied to the nodes of the top plate to compress the sample (U_z).
- An antisymmetry boundary condition (ZASYMM) about a the constant Z plane ($U_{x,y} = 0$, $R_z = 0$) was applied to all nodes within each fibre to simplify the compression simulations. This boundary condition removes any planar movements; thus the fibres only move in the thickness direction.

4.4.2.1.2 Material properties

The compression simulations were performed with the same material properties that were used in the peeling simulations, section 4.3.2. These properties are shown in Table 4.8.

Table 4.8 – Mechanical properties of the fibres

E1 (GPa)	E2	E3	ν12	ν13	ν23	G12	G13	G23
11.76	1.07	1.07	0.022	0.022	0.39	0.5	0.5	0.38

Defining specific inter-fibre bonds in a network-based material, such as paper, is a complex problem since locating all of the contact points in a random geometry requires a high level of network analysis. Therefore, the bonds in these simulations were defined using the **General_contact* definition in Abaqus. Using this feature, a contact point is created between any two surfaces that have a normal distance less than 1 µm. The inter-fibre bonds were modeled using spring elements with infinite elastic constant. This method provided a realistic distribution of the inter-fibre bonds in the microstructure of the paper samples during the compression, since the inter-fibre bonds were defined between each two surfaces that were closer than the corresponding distance value.

The compression simulations were performed at a constant displacement rate of 1 µm/s. The target compressed thickness was 100 µm (from a starting value of 450 µm), however, due to the complex morphology of the 3D meshed fibres, the FE simulations could not continue below about 200 µm thickness (each sample reached a unique thickness) because of the occurrence of a negative volume

error. Negative volume happens during large deformation simulations in finite elements when an element becomes so distorted that the volume of the element is calculated as negative. Therefore, the final thickness of the geometries was not equal, and each compression was performed up to the most possible step.

4.4.2.1.3 Stress Removal

At the end of the compression simulations, the fibres are highly stressed from the applied displacement. To eliminate this artificial state, a stress removal step was added. In this step, the deformed configuration of the compressed sample was exported out of Abaqus and then imported back into Abaqus in a zero-stress state. This resulted in removal of all of the accumulated stresses and strains. The advantage of this method is that the compressed nodal positions are retained while the mesh becomes stress-free. Unfortunately, this also resulted in a loss of all the inter-fibre bonds identified through the *General contact definition. Contacts in the tensile strength simulations were then re-formed manually using Abaqus CAE.

4.4.2.2 Tensile Deformation Step

The tensile deformation simulations were conducted to numerically calculate the tensile index of the low density paper samples with a mixture of softwood/hardwood fibres. The effect of mechanical and morphological properties of fibres, such as elastic moduli, length of the fibres, and basis weight were also studied using these simulations. The simulations were performed based on the samples that were compressed and exported in the zero-stress state as described in section 4.4.2.1. In order to calculate the tensile index of each sample, a displacement boundary condition was applied to a sample containing period boundary conditions. The boundary conditions and material properties that were used in these simulations are explained in the following sections.

4.4.2.2.1 Boundary Conditions

The uniaxial deformation simulations were performed using a rectangular frame. This frame, which was formed through simulation of 4 identical thin steel beams, was attached to the sample to generate periodic boundary conditions and apply the desired displacement to the sample. Figure 4.18 shows a schematic illustration of the movement of the frame that was used for the FE simulations. Note that the displaced beam in Figure 4.16 is not connected to the other beams and therefore they do not stretch.

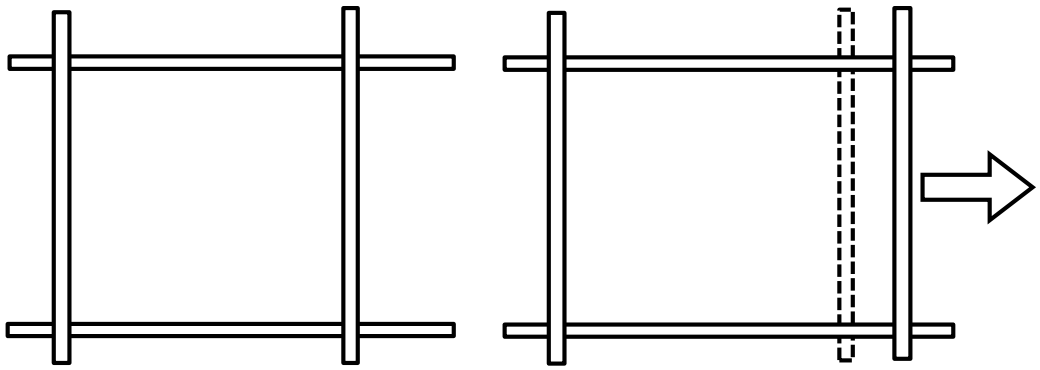

Figure 4.18– The schematic illustration of the movement of the frame

Note that each beam was connected to the sample where the fibres were touching the frame. Therefore, the fixed and displacement boundary conditions were applied to the frame instead of pulling the sample. The connection between the fibres and the beams were defined with the fully bonded contacts in the local contact areas that were defined manually between each fibre and the beam. An example of local contacts is shown in Figure 4.19 with the bright colour. The contacts algorithm and the material properties that were used for generating the local contact areas is explained in the next section.

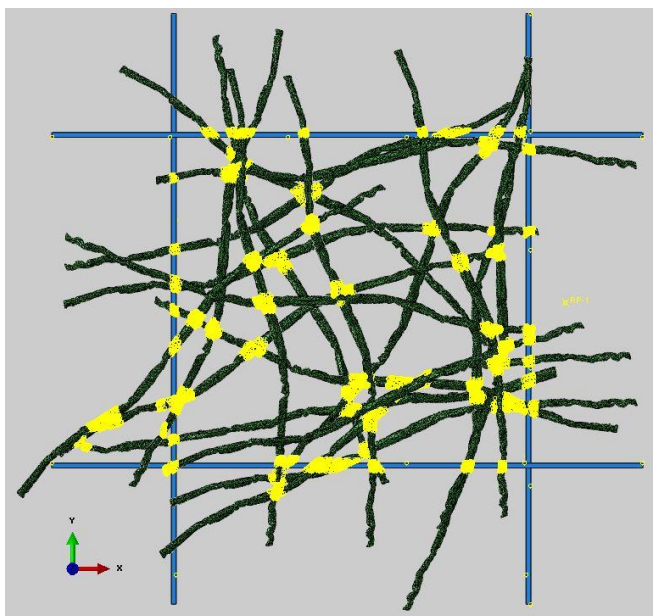

Figure 4.19 – The local contact areas of the

The specific boundary conditions used to create the uniaxial deformation simulation in ABAQUS software were as follows:

1. A fixed boundary condition was applied to the nodes of the left beam, avoiding any displacement or rotation. ($U_{x,y,z} = 0$, $R_{x,y,z} = 0$)
2. A horizontal displacement was applied to the nodes of the right frame beam to deform the sample (U_x).
3. An antisymmetry boundary condition (ZASYMM) about a the constant X plane ($U_{z,y} = 0$, $R_x = 0$) was applied to the nodes of the top and bottom beam to limit the motion of these beams to X-direction.

4.4.2.2.2 Material Properties

The inter-fibre bonds between the fibres were defined based on the local contact areas that were assigned manually. Since an import/export procedure was used to remove the compression stresses from the fibres, the contacts that were generated in the previous step were also removed from the sample in the export step. Therefore, a new contact pair was defined between each two fibres that were touching. This process was done manually by observing the 3D structure of the compressed fibres and determining the contact points. Each bond was defined through the following steps:

1. A local contact surface was defined for each fibre.
2. The bond was defined as a fully bonded contact pair using an elastic spring with infinity spring constant between the defined surfaces.

Using this procedure, fibre bonds were defined between the fibres that were in a closer normal distance of 1µm. The number of the bonds depends on the number of the fibres as well as the orientation of the fibres in the network samples. However, since the local contact surfaces were defined manually for each two fibres that were in contact, it is the number of the local contact surfaces that mainly determine the complexity of the simulations. Table 4.9 below shows the number of bonds and contact surfaces that were defined for each samples:

Table 4.9 – The number of the bonds and local contact surfaces in the tensile strength simulation geometries

	Mono-fibrous Samples				Mixture of Fibres					Simulations with various elastic modulus
	Long Fibres		Short Fibres		0%	14%	33%	60%	100%	
Number of bonds	11	33	28	60	11	23	24	21	28	33
Number contact surfaces	22	66	56	120	22	46	48	42	56	66

4.5 Summary

In this chapter, the methodology that was used for the simulation of the mechanical behaviour of an individual inter-fibre bond and the tensile strength of low density paper is explained. The fibre extraction process and formation of the simulation geometries was explained in the first part, and the boundary conditions, material properties and simulation steps of both groups of the simulations were explained in the second part. In addition, a novel fibre generation code that was used to form the low basis weight simulation geometries was also introduced. The results of both group of the simulations and a brief discussion on the simulation outputs are provided in the next chapter.

Chapter 5: Results and Discussion

The methodology that has been used to simulate the mechanical behaviour of an individual inter-fibre bond and the bulk properties of paper was explained in Chapter 4. In this chapter the results of both groups of simulations are presented and a discussion on the simulated findings is provided. In the first group of simulations, the behaviour of the inter-fibre bond was investigated based on the peeling behaviour of 7 bonded fibre pairs. In these simulations, the reaction force and the separation distance between the fibres were calculated from the unidirectional peeling of the inter-fibre bond. The results were then used to calculate the pre-failure dissipated energy of the bond. In the second group, the mechanical behaviour of the low-density paper samples was simulated. In this part, the displacement and reaction forces of the simulation geometries resulting from a uniaxial tensile stress were predicted. The simulation results were then used to calculate the tensile index of the geometries and to study the effect of the morphology of the fibres on bulk properties.

5.1 Bond Strength Simulations

Seven peeling simulations were performed to study the pre-failure behaviour of an individual inter-fibre bond. Figure 5.1 shows the local contact surfaces that were used in one of the peeling simulations. Based on the results of these simulations, the effect of the morphology of the NBSK fibres on the dissipated energy and fracture force of the bond was studied. In each simulation, an inter-fibre bond was formed between a pair of NBSK fibres. Examples are shown in Figure 5.2. The simulated fibres were meshed based on the scanned geometry of the actual NBSK fibres that were extracted from the scanned paper handsheets. The geometrical properties of the simulated fibres are listed in Table 4.3.

Table 5.1 – Dimensions of the fibres used in the peeling simulations

	Set 1	Set 2	Set 3	Set 4	Set 5	Set 6	Set 7
Length (µm)	1500	440	663	930	863	995	680
Equal Diameter (µm)	45	33	50	55	35	27	30

The peeling simulations were used to determine the effect of the diameter and length of fibres on the behaviour of the bond. This effect is shown in Figure 5.3. As can be seen, the maximum fracture force of the bond in these simulations was 5.25 mN (Set 4) and the minimum fracture force was 1.6 mN (Set 1). The maximum simulated dissipated energy of the bond was 102.8×10^{-12} kJ (Set 7) and the minimum dissipated energy of the simulated inter-fibre bond was 31.7×10^{-12} kJ (Set 1). The simulation results show that the fracture force of the simulated inter-fibre bonds decreased with increasing fibre length. Figure 5.4 shows the effect of the length and diameter of the fibres on the fracture fore of the inter-fibre bond. In this figure, the decreasing pattern of the fracture force is shown for two groups of fibres. It is shown that the fracture force of the inter-fibre bond in the simulations with more circular cross-sectioned fibres (Set 5, 6, 7) are higher than the ones with the fibres with a more collapsed cross section (Set 1, 2, 3). The same pattern was also seen for the dissipated energy of the bond, as can be seen in Figure 5.4. The cross section of the fibres of Set 1 and 5 are shown in Figure 5.5. This discrepancy in the simulation results can be explained by the difference between the moment of inertia of the cross section of the fibres, as a circular cross section leads to a relatively higher moment of inertia in comparison with the collapsed fibres with an oval shaped cross section. Eq. 5.1 and 5.2 sequentially show the equation of the bending deflection and the bending stiffness of the top fibre. Where P is the force that the bond applies to the top fibre at the contact point, L is the length of the fibre, E is the elastic modulus of the fibre, S is the bending stiffness of the beam, and I is the moment of inertia of the cross section of the fibre.

$$\delta = \frac{PL^3}{48EI} \tag{5.1}$$

$$P = S\delta \quad , \quad S = \frac{48EI}{L^3} \tag{5.2}$$

Based on the Eq. 5.2, the fibres with a relatively higher moment of inertia leads to a higher bending stiffness. It can be seen that based on the Eq. 5.1, the fibre with a higher bending stiffness will have a relatively lower deflection. The effect of the bending stiffness of the fibres on the bond strength calculations are further discussed in the next paragraph.

Figure 5.7 shows the contour of Mises stress in Set 2 just (a) before the initiation of damage and (b) after the bond was broken. As can be seen in this figure, the stresses found in the top fibre are highest just prior to failure. This stress increase in the top fibre can be mainly explained by analysis

of the bending deformation of the top fibre. Further, since the stress value of the elements at the local contact surfaces were used to define the damage initiation criterion for the cohesive behaviour in Abaqus, the failure of the inter-fibre was mainly controlled by the deformation of the top fibre. Therefore, beside the intrinsic strength of the bond, it is the bending stiffness of the top fibre that controls the behaviour of the bond. The bending stiffness of the top fibre can be explained using the bending of a cantilever beam with two pinned ends, Eq. 5.1 and 5.2. As can be seen in Eq. 5.2, higher values for the length of the beam decrease the bending stiffness and lead to lower reaction forces. Also, it can be seen that beams with lower moments of inertia have a lower bending stiffness. The top fibre in the peeling simulations represents a cantilever beam with two pinned ends, therefore, based on Eq. 5.1, relatively longer fibres with relatively smaller moments of inertia lead to lower bending stiffness and then lower fracture forces and dissipated energies. This analysis based on the concepts of mechanics of materials is in agreement with the simulation results provided previously, showing that the bending stiffness of the fibres has a significant effect on calculations of the strength of the inter-fibre bond.

As shown in Figure 5.2, the NBSK fibre have a complex morphology that can have twists, bends, or holes in the fibre wall. The behaviour of the inter-fibre bond is significantly affected by fibre geometry. Therefore, in order to understand the behaviour of the inter-fibre bond, it is necessary to study the effect of the morphology of the fibre on the behaviour of an individual inter-fibre bond. The results of the peeling simulation of the set 4, 5, 6, and 2 are used to investigate the effect of these parameters on the behaviour of the bond, as shown in Figure 5.6. It was seen that the peeling simulation of the inter-fibre bond between relatively longer fibres led to a lower bending strength and fracture forces. Also, the simulation of actual fibres resulted in a higher dissipated energy and fracture force for fibres with the relatively smaller diameters.

Figure 5.8 shows the stress concentration in one of the fibres of Set 1 of the peeling simulations. As can be seen in this figure, the stress value of the elements that are in a thinner section of the fibre is 10 times more than the other elements. Due to the complex morphology of the NBSK fibres, some sections of the fibre have relatively smaller diameters, creating high stress concentration. Clearly, the peeling simulations were affected by stress concentrations within the fibres, as a high stress value at one node may cause a singularity in the FE solution of the deflection of the beam.

The results of the peeling simulations of an individual inter-fibre bond were presented in this section. In these simulations, the actual geometry of the NBSK fibres was used to generate the simulation mesh. The results of the simulations were used to calculate the dissipated energy and fracture force of the inter-fibre, and to investigate the effect of the geometrical characteristics of the NBSK fibres on the strength of the bond. It is shown in this section that the morphology of the fibres, i.e. length and diameter, had a significant effect on the behaviour of the inter-fibre bond. Specifically, simulations with relatively longer fibres (Set 1, 4, and 6) and with bigger diameters (Set 1, 3, and 4) showed a lower dissipated energy and a lower fracture force during deformation of a fibre-fibre bond. Further, the results of these simulation showed that the morphology of the fibre has an important effect on the calculation of the fracture force and dissipated energy of the bond as the bending strength of the bond significantly changes the stress values at the contact elements. It is also shown that stress concentrations in the thin sections of the fibre changes the simulated behaviour of the bond. However, since the geometry of the simulated fibres were generated based on the imaging of the actual papermaking fibres, it is necessary to consider the differences between the simulated and actual morphology of fibres when the bond simulation results are compared with the experimental test results.

While the simulation results provided details about the peeling deformation of an inter-fibre bond, the simulation can be improved to describe the mechanical behaviour of the bond more realistically. In this thesis, the bond was defined based on a breakable elastic cohesive behaviour, however, an elasto-plastic model could be used to improve the accuracy of the simulations and to provide an estimation of the plastic response of the bond to the peeling loads. The free length of the fibre in the network of fibres, which is the length of the fibre between two contact points, is also shorter than the total length of the fibre. Therefore, comparison of the strength of the bond when the bond is formed between 2 individual fibres and the strength of an inter-fibre bond in the network of fibres can improve the understanding of the effect of the network on the strength of the bond.

The results of the peeling simulations provide a new insight on the mechanical behaviour of the inter-fibre bond. These results can be used to study the effect of the geometrical characteristics of the NBSK fibres on the behaviour of the bond. Further, the simulated fibre can be manipulated in the network simulation of the paper for tensile strength simulations. The provided methodology is

also useful for simulating the bonds between fibres in any simulation of the bulk behaviour of paper.

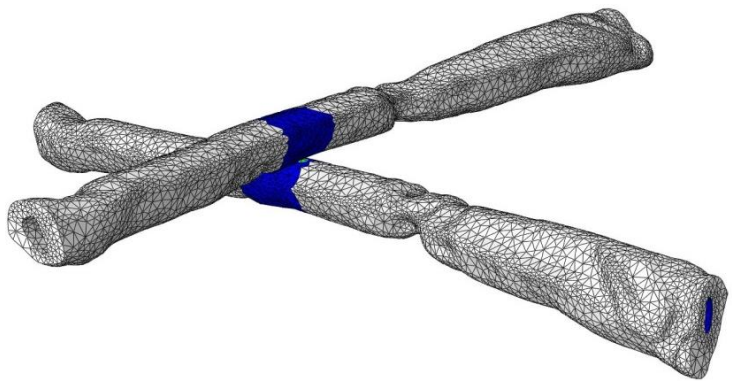

Figure 5.1 – Local contact surfaces of the simulated inter-fibre bond

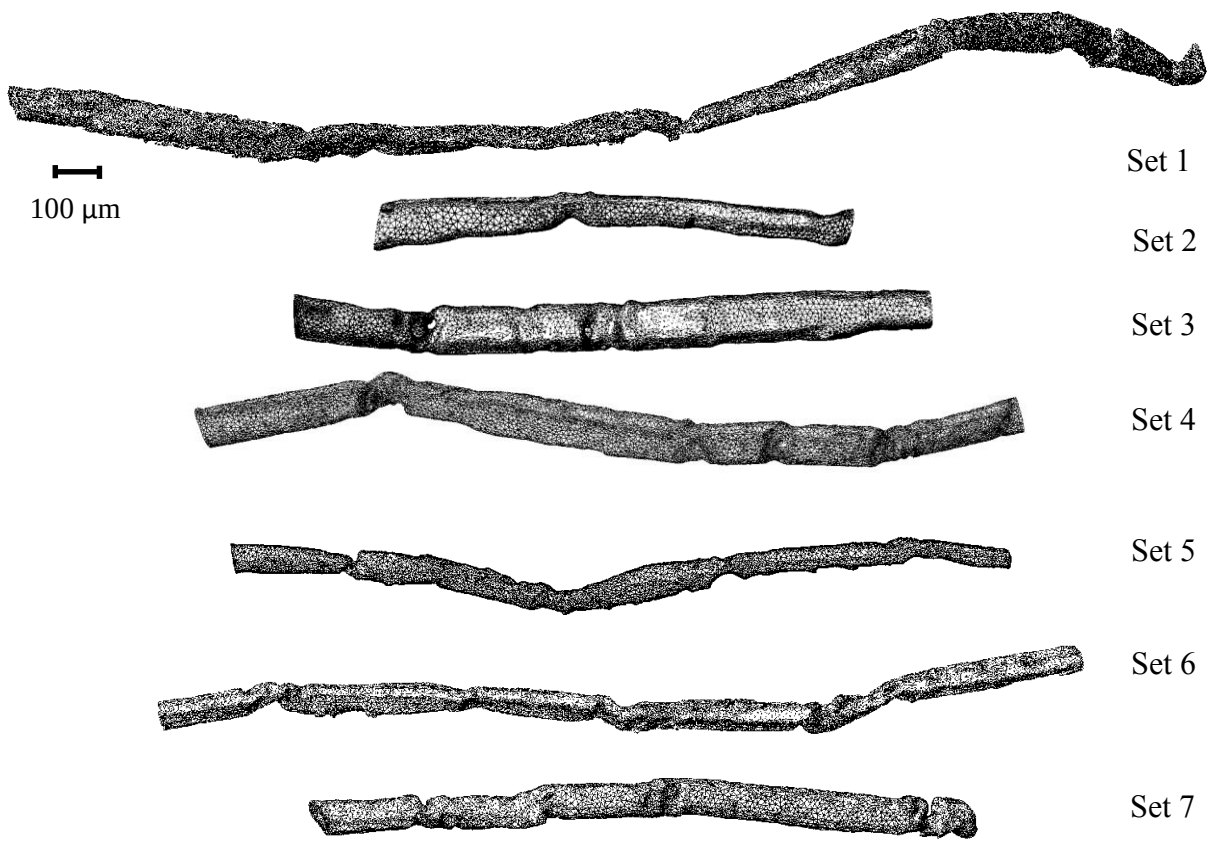

Figure 5.2 – Morphology of the tomography fibres used in the Bond Strength Simulations

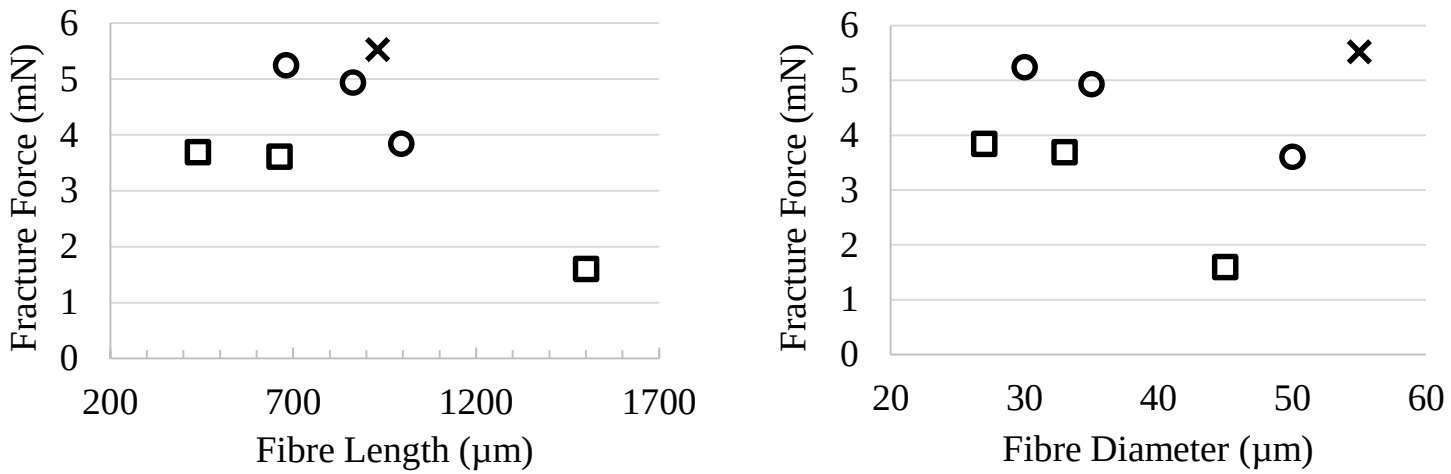

Figure 5.3 – The effect of the fibre's length (left) and fibre's diameter (right) on the fracture force of the bond

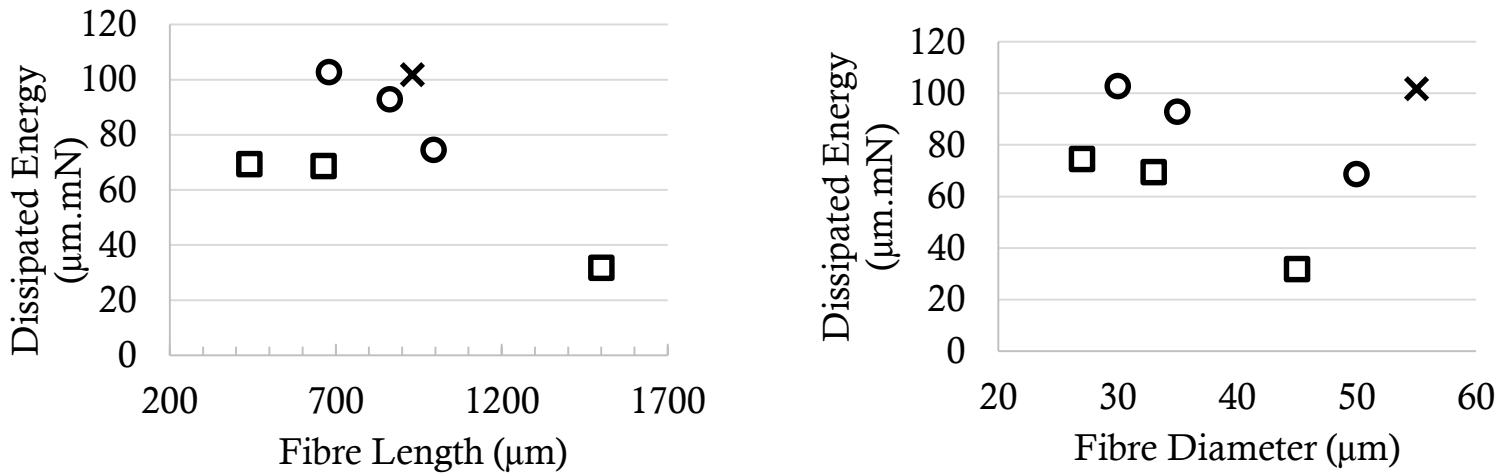

Figure 5.4 – The effect of the fibre's length (left) and fibre's diameter (right) on the dissipated energy of the bond

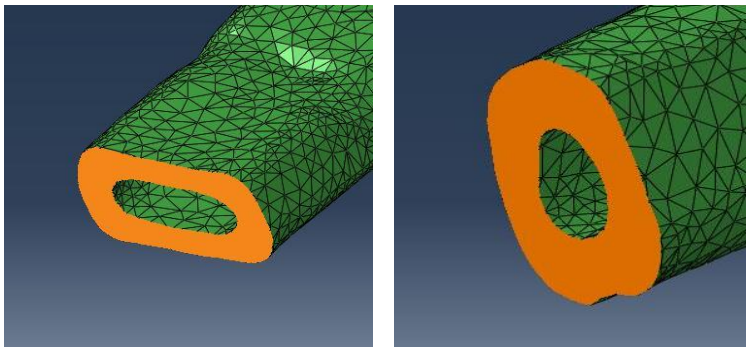

Set 3 Set 7

Figure 5.5 – Cross section of the fibres of Set 3 and 7 of the peeling simulations

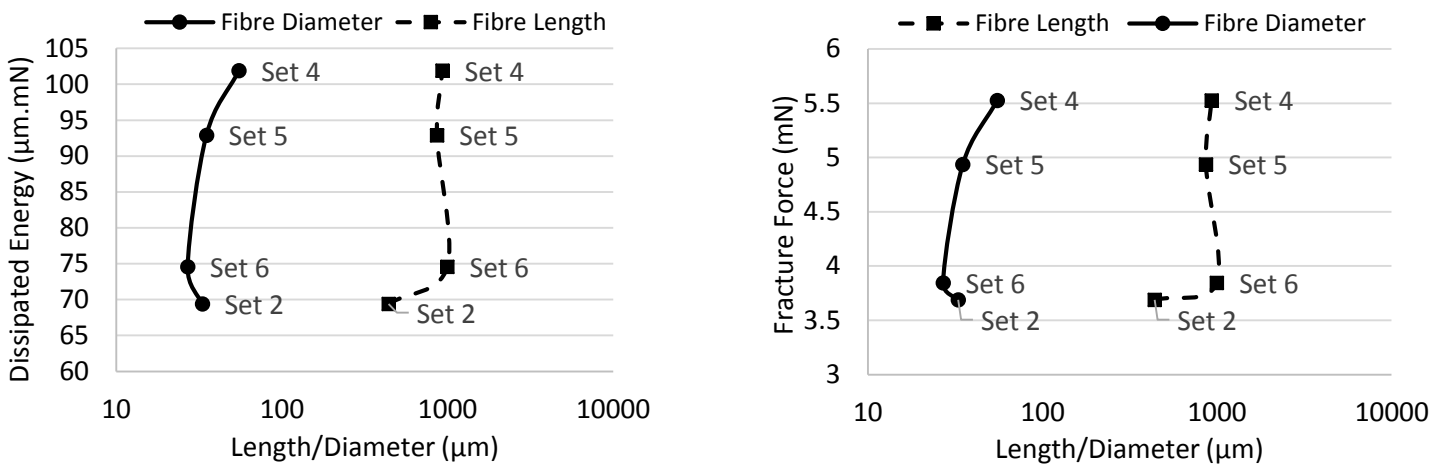

Figure 5.6 – Comparison between the effect of the diameter and the length of the fibre on the dissipated energy (left) and fracture force (right) of the bond

(a)

(b)

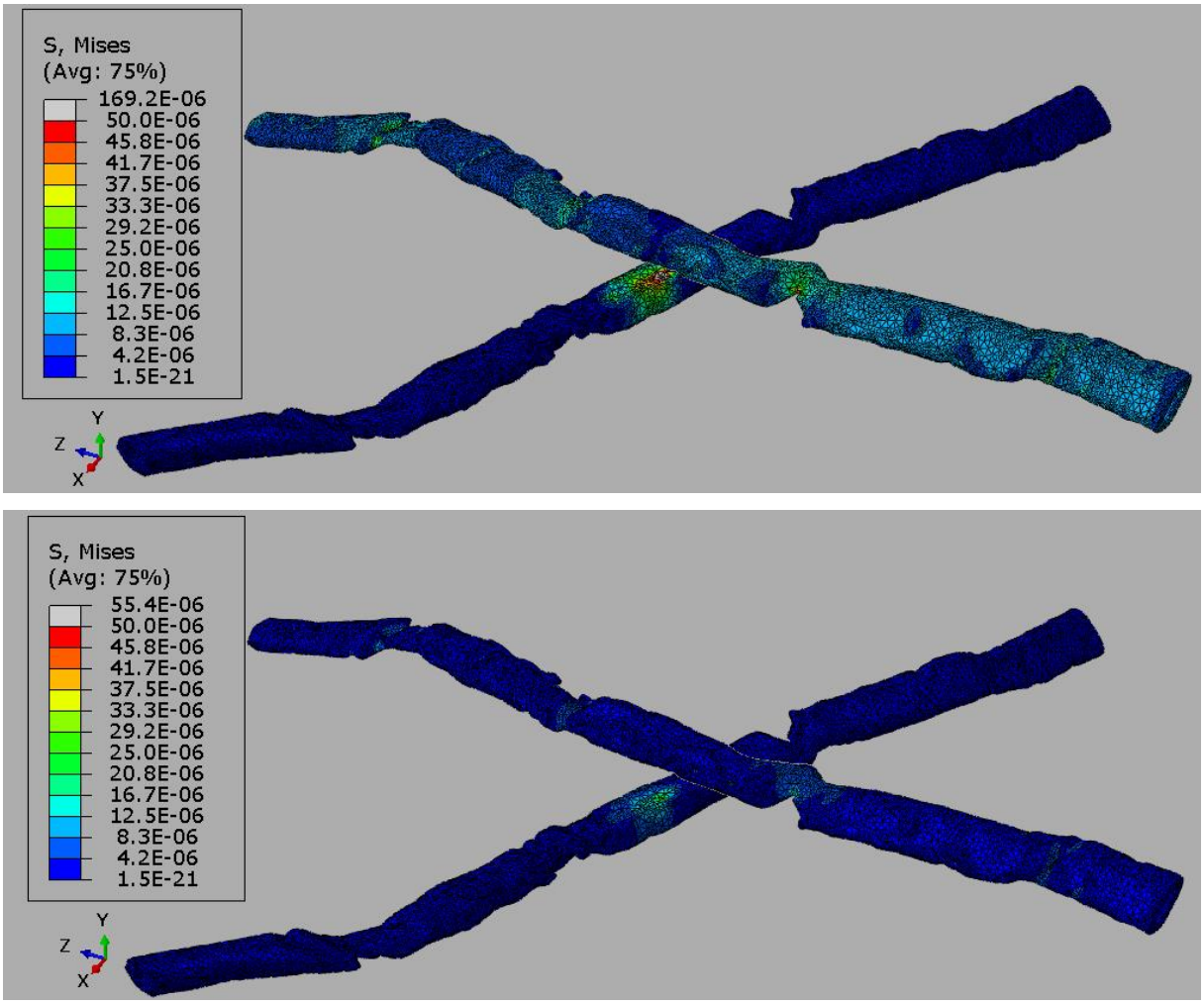

Figure 5.7 – The Mises stress contour (N/µm^2) (a) before the initiation of damage, (b) after the damage initiation

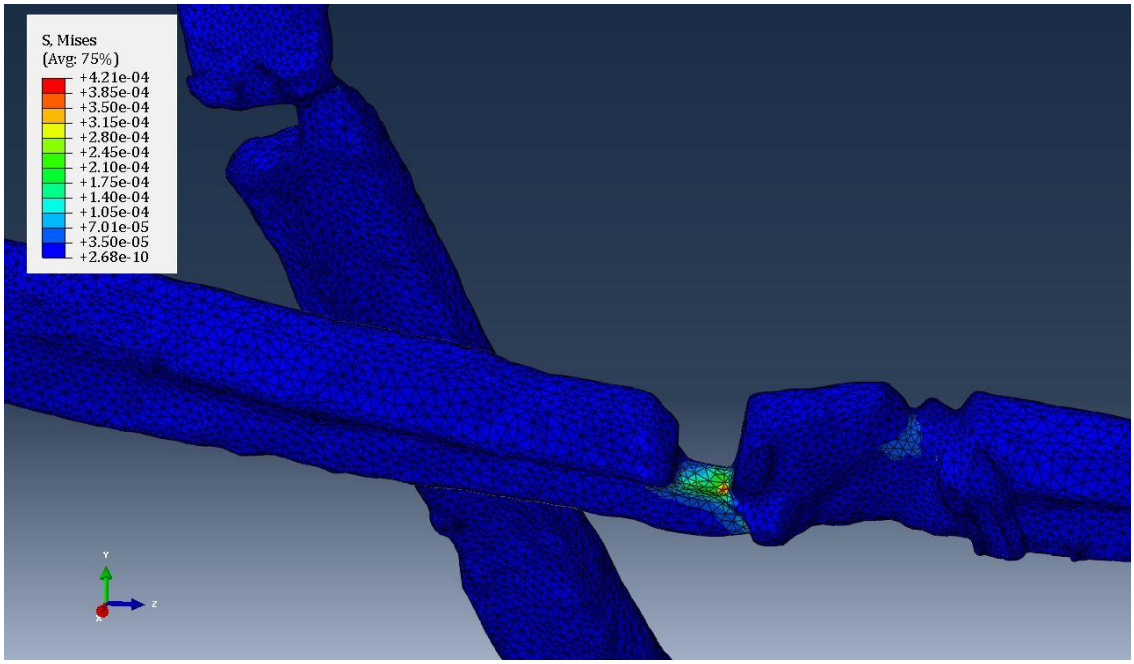

Figure 5.8 – Stress concentration (N/μm^2) in a the peeling simulations

5.2 Tensile strength simulations

Fourteen tensile strength simulations were performed using paper samples of various basis weights and fibre types. The simulations are categorized in four groups below, each showing the effect of one of the geometrical or mechanical properties of paper on the bulk properties of paper.

1. **The effect of fibre length and basis weight:** The tensile index of four mono-fibrous samples with various lengths and basis weights were numerically calculated to study the effect of the fibre's length on the bulk properties of the sample. Table 5.2 shows the basis weight and the fibre type for each paper sample.

Table 5.2 - Numerical simulations to study the effect of the fibre length and basis weight

Fibre type	Softwood fibre		Hardwood fibre	
Basis Weight (kg/m^2)	9.1	18.2	9.1	18.2

2. **The effect of the softwood/ hardwood mixture:** In order to study the effect of the mixture of various fibre types on the tensile index of paper, the mechanical behaviour of five simulation geometries with various mass percentages of hardwood (short) fibres were simulated. Table 5.3 shows a list of the mass percentage of hardwood fibres, basis weight, and the percentage of the number of hardwood fibres in each sample.

Table 5.3 - Numerical simulations to study the effect of the mixture of softwood/hardwood

Mass percentage of the hardwood content (%)	0	14	33	60	100
Percentage of the hardwood fibres (%)	0	25	50	75	100
Basis Weight (kg/m^2)	18.41	16.07	13.73	11.40	9.06

3. **The effect of the elastic moduli:** Three different values of the fibre's Young's modulus were used to study the effect of the mechanical properties of the fibre on the tensile index of paper. In these simulations, the deformation of a mono-fibrous (softwood) paper sample with a basis weight of 18.1 kg/m^2 was simulated to study the effect of the material properties of the fibre on the bulk properties of paper. The material properties that were used in these simulations are listed in Table 5.4.

Table 5.4 – Elastic material properties of the fibres

E_1 (GPa)	E_2	E_3	ν_{12}	ν_{13}	ν_{23}	G_{12}	G_{13}	G_{23}
4.50	0.41	0.41	0.02	0.02	0.39	0.20	0.20	0.15
11.76	1.07	1.07	0.02	0.02	0.39	0.51	0.51	0.38
23.23	2.11	2.11	0.02	0.02	0.39	1.01	1.01	0.76

4. **Samples with cylindrical fibres:** In order to study the effect of the actual morphology of the papermaking fibres on the bulk properties of paper, the tensile index of two samples with cylindrical fibres were numerically calculated and compared with the results of the simulations with actual morphology of papermaking fibres. The physical characteristics of the cylindrical fibres are listed in Table 5.5.

Table 5.5 - Numerical simulations to study the effect of the mixture of softwood/hardwood

	Sample 1	**Sample 2**
Number of cylinders	10	20
Number of Bonds	12	26
Basis weight (g/m^2)	10.82	21.63

The simulations were performed using eight parallel processors and 16 GB of memory (RAM). Each tensile strength simulation was performed in less than 60 minutes, however, compression simulations and manual bond generation steps were performed prior to the final tensile test simulations. It was observed that the calculations cost of the tensile strength simulations was dramatically increased by an increase in the basis weight/ or number of the fibres that form the simulation geometry. It was seen that the calculations of the tensile strength simulation of the geometries with a basis weight of 40 g/m^2 can take more than a week to be performed with the mentioned simulation setup. Due to the limited memory of the simulation setup, higher basis weights lead to simulation errors, which makes these simulations impossible.

5.2.1 Simulation results

The results of the tensile strength simulations are explained in this section. Figure 5.9 shows the original and deformed morphology of one of the tensile strength simulation geometries. As can be seen in this figure, the simulation geometries were deformed using a uniaxial displacement that was applied to the moving frame in the x-direction. The frame, which was attached to the geometry, was fixed in one end and a displacement was applied to the other end of the frame using a reference point. The reference point was attached to the moving bar of the frame, which enabled the application of the displacement boundary condition on a single point.

In these simulation, the reaction forces and the displacements of the reference point in the x-direction was reported, which represents the displacement and the reaction force of the sample. These simulations were then used to calculate the Rupture Index (RI) of the simulation geometry, as shown in Equation 5.2.

$$RI = \frac{F_{max}}{BW \times W} \tag{5.2}$$

where F_{max} is the maximum reaction force of the tensile strength simulation, BW is the basis weight of the simulation geometry, and W is the width of the frame. The rupture index is usually presented in units of kN.m/kg.

5.2.1.1 Effect of Basis Weight

The effect of basis weight on the rupture index of paper is presented in Figure 5.10. This figure shows the result of the tensile strength simulation of geometries that were formed based on softwood and hardwood fibres. As shown in the figure, the basis weight has a major effect on the rupture index of the paper, the tensile strength simulation of the geometry with a basis weight of 18.2 g/m^2 lead to a rupture index of 6.8 kN.m/kg for hardwood fibres, and 26.5 kN.m/kg for softwood fibres. Similarly, a basis weight of 9.1 g/m^2 lead to a rupture index of 19.5 kN.m/kg for hardwood fibres, and 35.7 kN.m/kg for softwood fibres. It is shown that although the higher basis weights result in lower rupture index, the geometries that were formed mostly with softwood (longer) fibres have relatively higher tensile index compared to the geometries that were formed with hardwood (shorter) fibres.

5.2.1.2 Effect of the Young's modulus of the fibre

The effect of the elastic modulus of the fibre (E_f) on the mechanical behaviour of paper was studied in three simulations. In these simulations, the response of a geometry having a basis weight of 18.1 g/m^2 to a tensile deformation was studied. Three different Young's moduli values were used for the fibres, as explained in section 5.2. Figure 5.11 shows the effect of the elastic modulus on the rupture index. It is shown that a rupture index of 52.4 kN.m/kg was calculated from the simulations of the tensile deformation of the geometry with the elastic modulus of 23 GPa, but a rupture index of 10.2 kN.m/kg was calculated from the simulation of the same geometry with the elastic modulus of 5 GPa. As it can be seen in Figure 5.11, this simulation was also performed with an elastic modulus of 11 GPa, and it is shown that the elastic modulus of the fibre linearly changes the bulk mechanical properties of paper. This linear relation between the elastic modulus of the fibre and the bulk properties of paper has been previously predicted in the literature, such as the work of Page, et al. [38] as explained in section 2.5.1. As expected from Page's constitutive model, the simulation results show that the rupture index of the simulated geometries were linearly dependent on the elastic modulus of the fibres that were used to form the geometry.

5.2.1.3 Effect of the actual morphology of NBSK fibres

The effect of the actual morphology of the NBSK fibres on the rupture index of the low density paper is presented in Figure 5.12. In this figure, the results of the tensile strength simulation of both geometries that were formed based on the actual geometry of the NBSK fibres and simple cylindrical fibres are shown. As can be seen in the figure, the simulation of the tensile strength of the geometries that were formed with simple cylindrical fibres and with a basis weights of 10.8 g/m^2 and 21.6 g/m^2 respectively lead to rupture indexes of 13.4 kN.m/kg and 4 kN.m/kg.

The morphology of the fibres has a significant effect on the rupture index of the simulated paper geometry. As shown in Figure 5.12, the rupture index of the geometries that were formed based on the cylindrical fibres were smaller than the similar geometries that were formed with the actual morphology of NBSK fibres. In these simulations, an attempt was made to create simulation geometries with the same basis weights, however, due to the mass difference between the NBSK fibre and cylindrical fibre, significant differences can be seen.

The discrepancy between the results can be explained by the following factors:

1. The number of contact points in the geometry of cylindrical fibres was lower than the NBSK fibres. As it can be seen in Figure 5.12, the simple straight geometry of the cylindrical fibres resulted in less contacts between the fibres, reducing tensile strength.
2. The morphology of the NBSK softwood fibre that was used to form the simulation geometry has kinks and curls. Therefore, the geometry was pre-deformed to a greater extent as compared to the cylindrical fibres prior to application of the tensile deformation.

5.2.1.4 Effect of hardwood/softwood mixtures

The effect of mixing hardwood and softwood fibres on the strength of paper was numerically studied using the FE simulations. Figure 5.13 shows the hardwood/softwood mixture simulation geometries with the 14% and 25% of hardwood content. In these simulation the reaction forces of paper samples that were formed using the actual morphology of papermaking fibres was numerically measured, as shown in Figure 5.15. As can be seen, the rupture force of the generated simulation geometries decreased as the percentage of hardwood (relatively shorter) fibres were increased. While a rupture force of 644 mN was measured for the simulation geometry that were formed with 100% softwood fibres, a rupture force of 232 mN was measured for the 100% hardwood simulation geometry.

The simulated reaction forces were then used to calculate the rupture index of the simulation geometries. A rupture index of 26.4 kN.m/kg was calculated for a simulation geometry with 14% of hardwood content, while a rupture index of 16.7 kN.m/kg was simulated for the geometry that was formed with 60% of hardwood fibres. As can be seen in Figure 5.15, the simulated tensile index of paper samples with relatively lower hardwood fibres were higher than the geometries with higher hardwood fibres.

As discussed in section 2.4 and 2.6, the experimental and numerical simulations have shown that the paper samples that were formed with relatively longer fibres often have higher mechanical strength characteristics. It is shown in these numerical simulations that as the softwood content of the simulation geometry were decreased, the corresponding rupture force and tensile index of the geometry was decreased. As the mass percentage of the hardwood fibres has a direct effect on the basis weight of the samples. A uniform pattern was expected from the numerical simulations. However, the simulation results didn't show a direct relation between the mass percentage of the hardwood fibres and the tensile strength of the geometry, which can be explained with the following parameters.

- The simulation geometries were formed by artificially compressing the NBSK fibres. The final amount of the compression in these simulations was limited by the quality of the mesh and the available computational resources. In some of the simulations, the geometry was of greater thickness than the actual paper samples, leading to fewer bonds.
- In these tensile strength simulations, the behaviour of the geometry was only studied in the elastic region as the fibres were assumed to have elastic material properties. The pre-failure elastic-plastic defamation effects were not considered in the simulations
- While the microstructure of paper includes a wide range of fibres with various morphological characteristics, the simulation geometries were formed using two NBSK fibres to simplify the simulations. Therefore, the effect of the short fibres and fibre entanglements were not considered in the sample.
- The mass percentage of the hardwood fibres in the actual paper samples is often measured by measuring the statistical percentage of the fibres that were used in the production process. However, an exact mixture percentage can be reached in the numerical simulations leading to difference between the experimental and numerical results.

In this thesis, the response of the NBSK fibres of the paper geometry to a tensile deformation was numerically simulated. Since local contact surfaces between the fibre pairs were used to define the inter-fibre bonds through the network of fibres, the total displacement boundary condition of the frame generated various modes of loadings, such as bending, axial deformation in the fibres. Therefore, these simulations were able to provide a more realistic estimation of the bulk properties of paper as well as the response of the network of NBSK fibres to a uniaxial deformation.

Figure 5.17 shows an example of the bending of the fibre when the network is deformed. In this figure, the deformation of an individual fibre is shown while the fibre is isolated from the network. As it can be seen in this figure, the fibre is bent in couple of section by the contacts that it has with the other fibres. This shows the effect of the number of bonds on the strength of the fibre, since with an increase in the number of the bonds the length of the free section of the fibre decreases. Correspondingly, this increases the bending strength of the fibre.

Figure 5.16 shows the contour of Mises stress in the deformed geometry of softwood fibres with a basis weight of 18.2 g/m^2. The simulated geometry had the highest basis weight and longest fibres between the simulations, which increases the probability of the fibres that were connected to both sides of the frame. Therefore, some of the fibres were highly deformed when the displacement boundary condition was applied in the x-direction and to the right side of the frame. As can be seen in this figure, the highest stress values were generated in these fibres that were mainly axially stretched. Although the stress value of the elements in the axially deformed fibres reached the maximum value of 6.2 GPa, the average stress value of the elements of the other fibres was 6 MPa. Therefore, the axial strength of the fibres significantly affects the simulated bulk strength of the geometry. However, it should be mentioned that the tension strength of the fibres should not be considered as one of the properties that affect the bulk strength of paper as this phenomenon only occurs in the numerical simulations with a small size geometry. Tensile deformation of fibres can also be seen in the actual experimental tensile strength test of paper, but the actual papermaking fibres are much shorter than the length of the sample and the fibres are not connected to the both sides of the sample.

5.2.2 Validation of the results

A comparison between the simulation results and results of the previous experimental tensile strength tests on paper handsheets in the literature were used to validate the tensile strength simulations. I'anson et al. [74] have presented results of the tensile strength tests on paper handsheets that were generated from pine fibres with basis weights of 5 - 200 g/m^2. Tensile strength tests were carried out on 15 mm wide strips between jaws of 100mm apart. In this study, the results of tensile strength tests were used to study the effect of the basis weight on the tensile index of the handsheet. These test results were used in this project for validation of the simulation results. As can be seen in Figure 5.18, the simulation results were in a an agreement with the tensile strength test results. However, unlike I'anson's experimental test results, the simulation results do not show an increasing rupture index with increasing basis weight. This discrepancy may be due to the fact that the thickness of the simulation geometries was much thinner as compared to the actual geometry of paper. Up to the best of the author's knowledge, the variation in the pattern of the tensile index is generated from the error in the thickness and number of the bonds of these geometries.

The results of the experimental tensile strength tests that were performed at the Pulp and Paper Center of UBC Vancouver campus were also used to validate the numerical simulations. A comparison between the calculated rupture index of the FE simulations and the experimental tensile strength testing of paper samples that were formed based on a mixture of NBSK fibres is shown in Figure 5.19. While the experimental test results lead to a rupture indexes of 28 kN.m/kg for a 40 g/m^2 paper sample, the FE simulation resulted in a rupture index of 26.5 for the 18.4 g/m^2 simulation geometry. As it can be seen in Figure 5.19, the range of the calculated rupture index of the simulated geometries was in a good agreement with the experimentally measured tensile index of the actual paper. However, point to point comparison of the rupture indexes were not possible due to the differences between the basis weights of the simulations and the actual paper. Since the size of the simulation mesh had an important effect on the calculation cost, as explained in section 4.4.2.3, the simulations were only performed for the geometries with a maximum basis weight of 18.5 g/m^2. Moreover, basis weights lower than 40 g/m^2 could not be reached for the samples that were generated for the experimental tensile strength tests.

The rupture index of the simulations were affected by the number of the inter-fibre bonds in the geometry. As it is shown in Figure 5.19, the rupture index of the simulation geometries was

decreased first and then increases according to the basis weight, which can be explained by number of the bonds in the geometry. Table 5.6 shows that the number of the inter-fibre bonds in the simulation geometries with 14% and 33% of hardwood content were less than the number of the bonds in the other simulations. Therefore, the fibres were able to bent or stretched more in these geometries, which lead to a lower strength and rupture index. The number of the inter-fibre bonds has a significant effect on the tensile strength of paper, as paper samples that were formed with longer fibres often have a higher number of bonds and a higher tensile strength, as discussed in section 2.6.2. However, it should be mentioned that due to the high calculation costs the size of the geometries that were simulated in this section were smaller than the usual paper samples that were used for the tensile strength samples and the bonds were manually formed between each two fibres that were within a distance of 1μm.

Table 5.6 – Number of the inter-fibre bonds in the simulation geometries

Mass percentage of the hardwood content (%)	0	14	33	60	100
Number of the bonds	26	20	20	24	26

5.2.3 Discussion

The results of the tensile simulations of the low density geometries of NBSK fibres has been presented in this section. In these simulation, the effect of the morphology of the NBSK fibre on the rupture index of paper was studied. It has been shown in section 5.2.1.2 that based on the simulation results, the paper handsheets that are formed with the fibres with a higher elastic modulus will provide better mechanical properties, such as the elastic strength. Further, the simulation results showed that the elastic modulus of the fibre linearly affects the bulk rupture index of paper.

Although the geometry that was used in the literature for the simulation of the strength of paper was often formed using the simplified cylindrical fibres, in this thesis, actual morphology of the NBSK fibres were used to form the simulation geometries. A comparison between the simulation results of two similar geometries with the actual NBSK fibres and cylindrical fibres was also presented in section 5.2.1.2. Based on these simulation results, it has been shown that the rupture index of the geometry of the simplified fibres were lower than the geometry of the actual NBSK fibre. Therefore, the simulation of the behaviour of paper using a simplified geometry of the fibres, such as cylinders, cubes cannot accurately estimate the mechanical properties of the fibres and

leads to a lower value of the tensile index of paper. In contrast to the actual morphology of the NBSK fibres that is bend, twisted and has various diameters along the fibres, the cylindrical fibres are straight without any bends, therefore, the simulation geometry that was formed based on cylindrical fibres also had less number of the inter-fibre bond.

In the last part, the results of the simulations of the geometries that were formed based on a mixture of the hardwood and softwood fibres were presented. Based on the simulation results, it has been shown that the mechanical strength of the paper is decreased when the percentage of the hardwood fibres in the geometry is increased. The results of these simulations show that the paper handsheets that were generated with a hardwood/softwood mixture have a relatively lower mechanical strength compared to the handsheets that were formed from NBSK fibres. In order to maintain the basis weight of the sample, the total number of the fibres will change when hardwood (shorter) fibres are added to the sample, however, in this project, the total number of the fibres were constant for all of the mixture geometries and the basis weight of the geometry changes. Further, a comparison of the results of the simulations and experimental testing of actual paper handsheets were provided which showed a good agreement between the rupture index of the simulated geometries and the tested paper.

The tensile strength simulations provide a detailed understanding of the mechanisms happening in the microstructure of paper and between the papermaking fibres. The simulations can be used to determine the local stresses in each fibre as well as the bulk mechanical properties of the fibres. The simulations also provide a straight forward methodology to study the mechanical behaviour of paper under various loading conditions, the simulations.

Although the numerical tensile strength simulations provide new insights over the effect of the geometrical properties of NBSK fibres on the bulk properties of paper, the following improvements would provide a more realistic estimation of the mechanical strength of paper:

- Larger simulation geometry can be used for the tensile strength simulations to include the random orientation of the fibres in the simulations. In this thesis, the calculation cost of the simulations geometries limited the size of the simulation geometry, therefore, simulation geometries that were used in the tensile strength simulations had a max basis weight of 18.2 g/m^2 and maximum number of 40 fibres. Since the actual microstructure of paper is formed based on a random network of fibres, simulations with more fibres can provide more realistic estimation of the behaviour of paper.

- Elastic breakable inter-fibre bonds can be used in the tensile strength simulations. The fully bonded contacts that were used in the tensile strength simulations of this thesis can be updated with a cohesive breakable bond. The breakable bond can be defined based on the local stresses at the fibres. Therefore, the tensile strength simulations can be continued up to the failure of the geometry.
- Plastic material properties of the fibres can be considered in the tensile simulations to study the plastic deformation of the paper. In this thesis, only the elastic deformation of the paper is studied, however, the plastic and permanent pre-failure deformation of the paper can be simulated if the plastic material properties of the fibre are considered in the simulations.

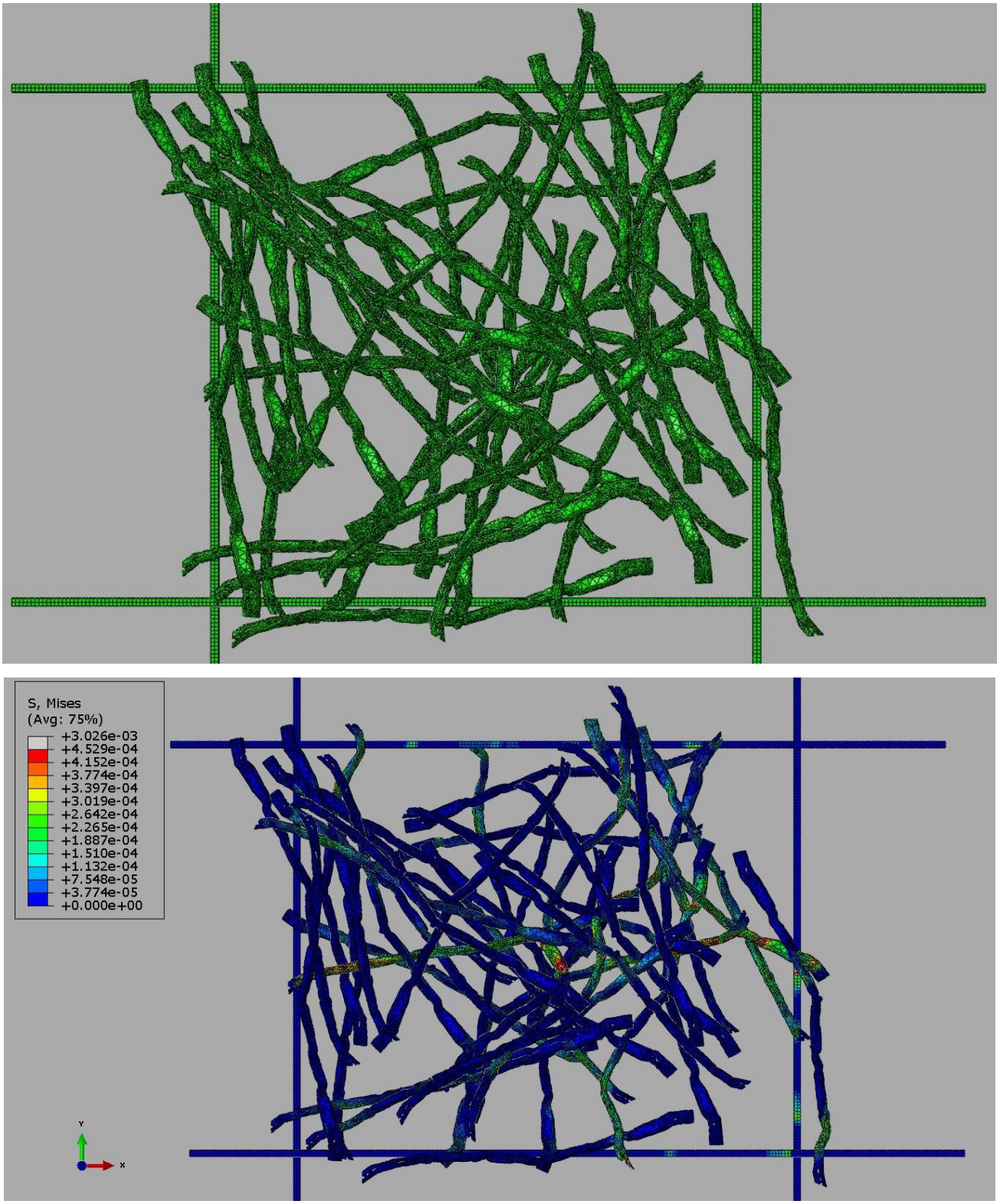

Figure 5.9 – The original geometry (left) and the of contour of Mises stress (N/μm^2) (right) of the deformed geometry of a tensile strength simulation

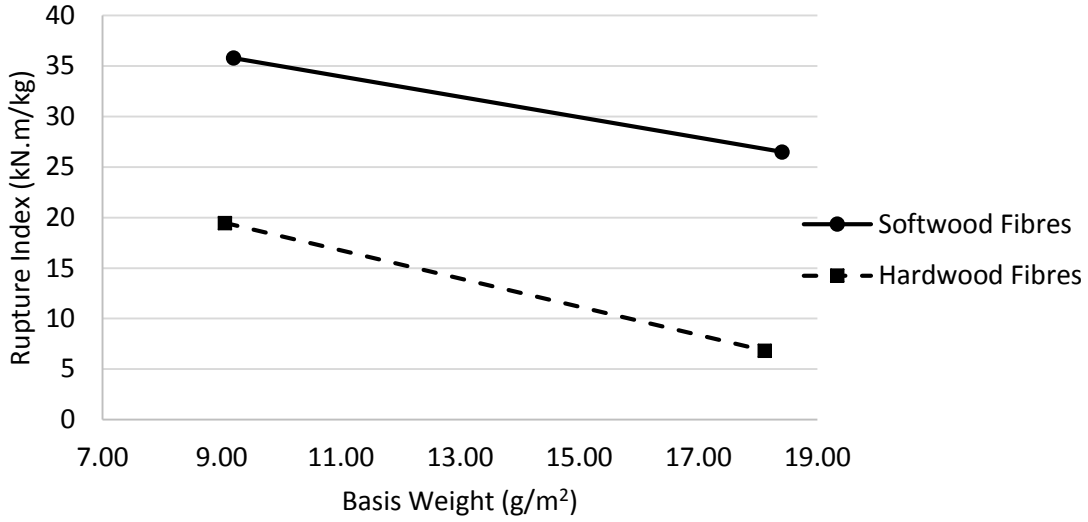

Figure 5.10 – The effect of the basis weight on the rupture index of low density paper

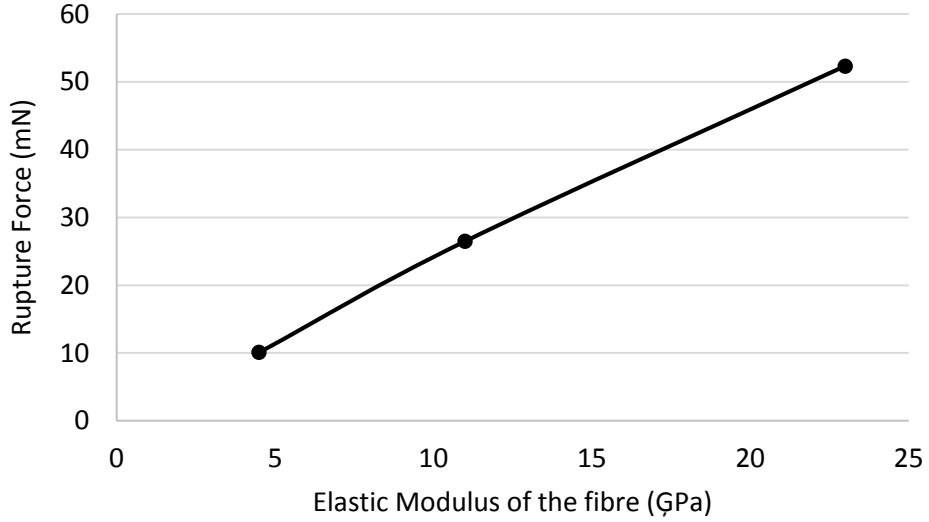

Figure 5.11 – The effect of the Young's modulus of the fibre on the rupture index of paper

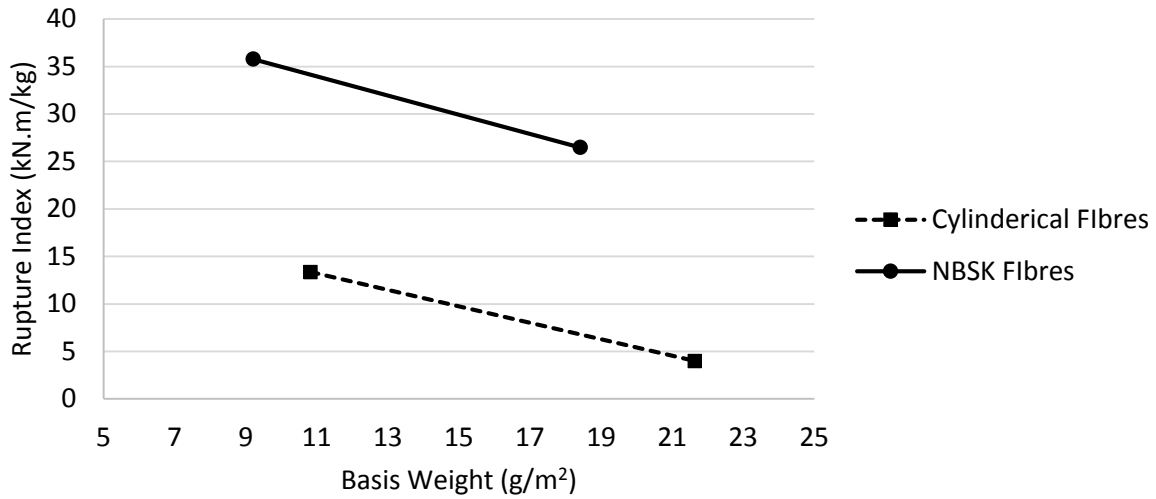

Figure 5.12 – The effect of the morphology of fibres on the rupture index of low density paper

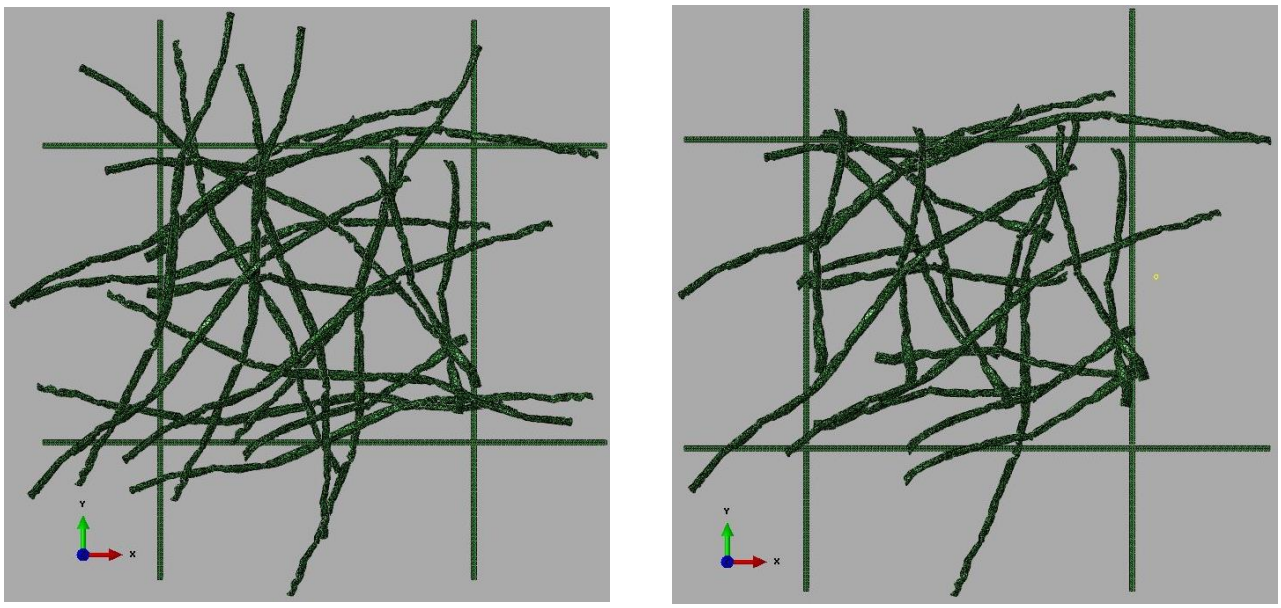

Figure 5.13 – The tensile strength simulation geometries with 14% of hardwood fibres (left) and 60% of hardwood fibres (right)

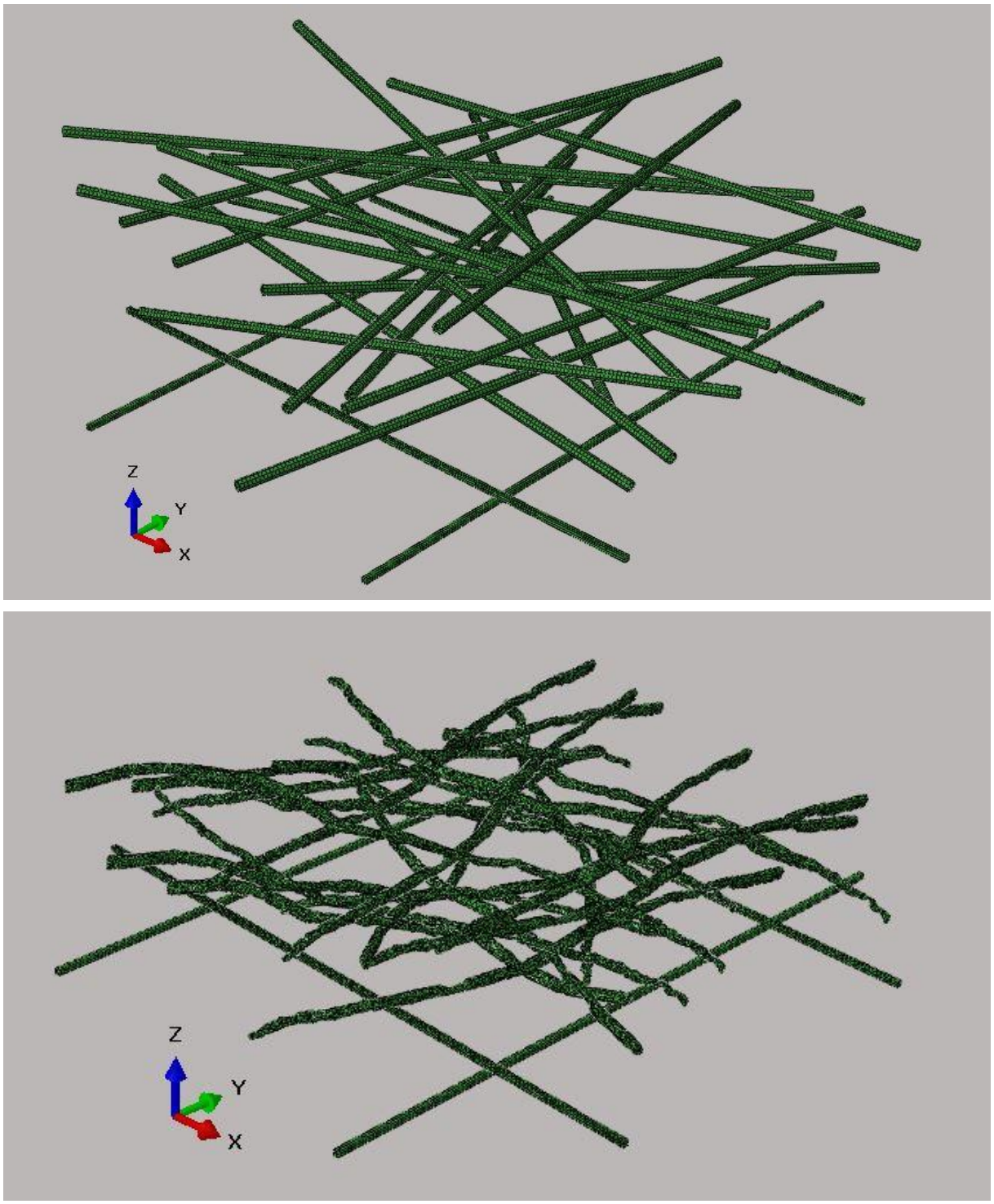

Figure 5.14 – The simulation geometry of cylindrical fibres (top) and actual NBSK fibres (bottom)

Figure 5.15 – The effect of the mixture of hardwood fibres on the rupture index of paper

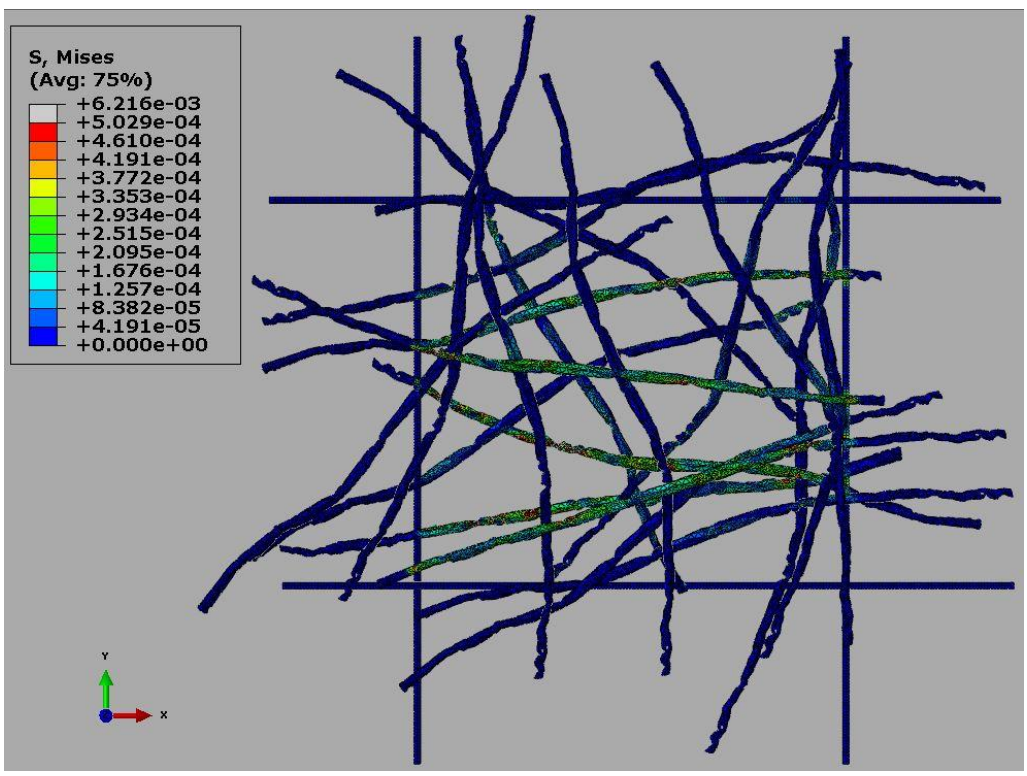

Figure 5.16 – Contour of Mises stress (N/μm^2) of the deformed geometry of NBSK fibres

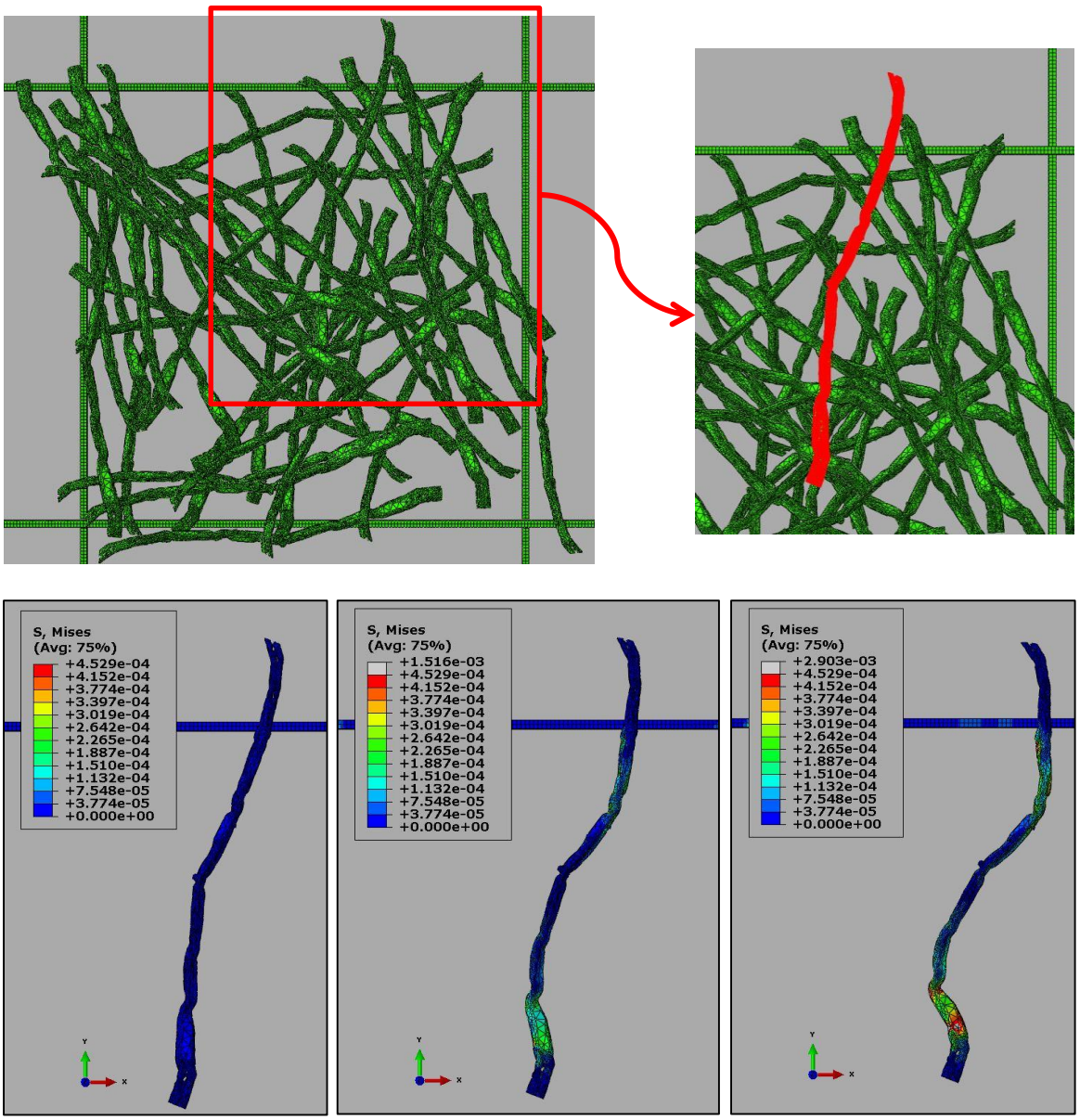

(a) (b) (c)

Figure 5.17 – The bending deformation of an individual fibre (isolated from the geometry) in the (a) original state, (b) half deformed, (c) final deformation

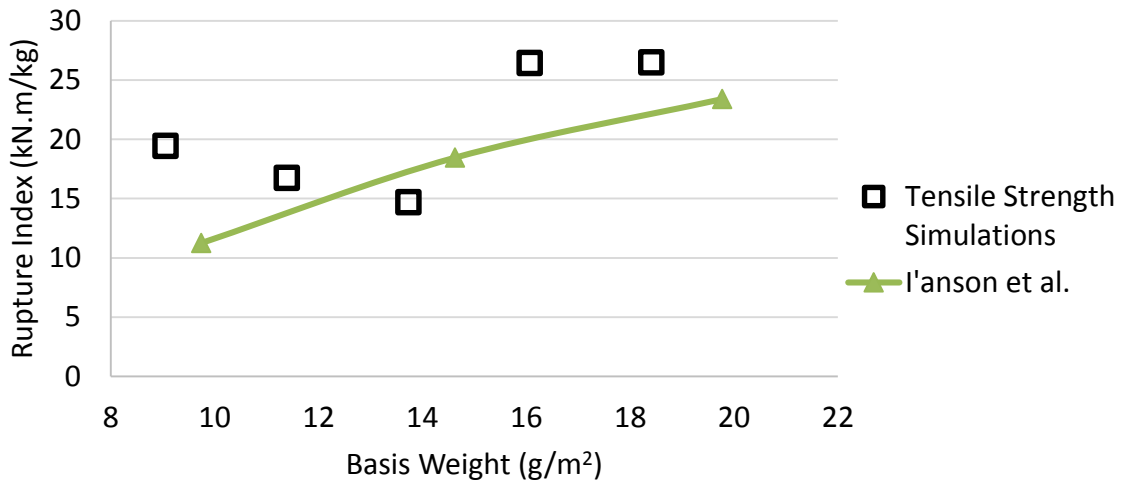

Figure 5.18 – Results of the tensile strength simulations vs experimental tests

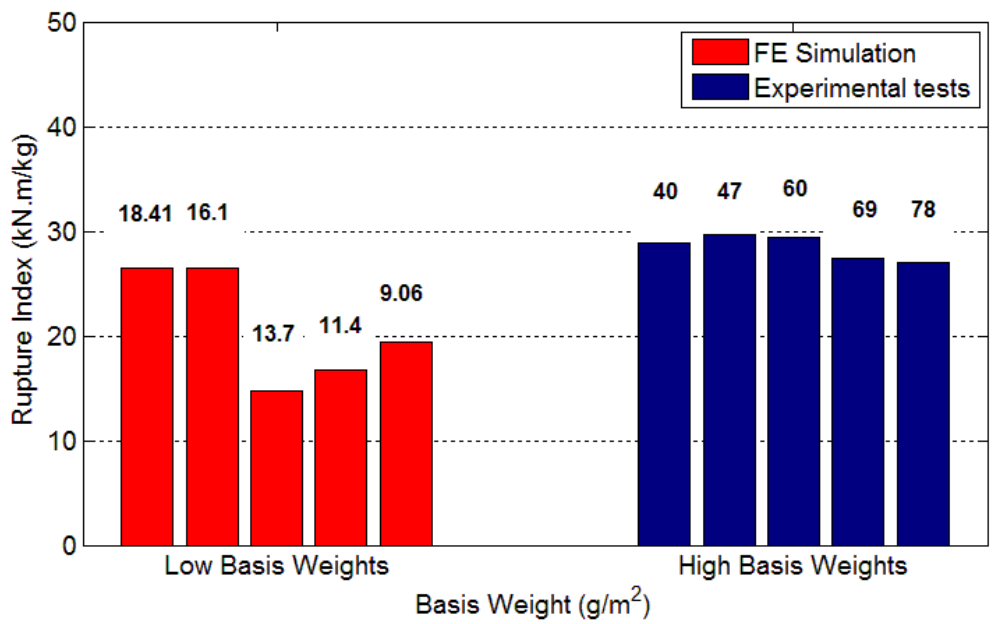

Figure 5.19 – The rupture index of paper samples with various basis weights

5.3 Summary

The results of both groups of peeling and tensile strength simulations were presented in this section. In the first part, the pre-failure behaviour of an individual inter-fibre bond was simulated based on the actual geometry of NBSK fibres. The results of the peeling simulations were used to investigate the effect of the morphology of the NBSK fibres on the dissipated energy and fracture force of the inter-fibre bond. In the second part, the results of the tensile strength simulations were presented. In this part, the response of the simulation geometries to a uniaxial displacement was presented. The simulation results were used to calculate the rupture index of the simulation geometry and study the effect of the basis weight, elastic modulus of the fibre, and the actual morphology of NBSK fibres on the rupture index of paper. The simulation results were also compared to the experimental results.

Chapter 6: Conclusions

Numerical simulation methods such as Finite Element Method (FEM) are recently used to simulate the tensile deformation of paper. Accurate estimation of the geometry of the papermaking fibres have been recently used to prepare the meshed geometry of the FE simulations to study the effect of the geometrical properties of papermaking fibres on the strength of paper. These simulations can be also used to study the parameters that affect the strength of paper, such as the strength of the papermaking fibres and the inter-fibre bonds. Although the current simulation methods have been used to determine how the strength of the fibres effect the strength of paper, none have used the actual morphology of fibres to develop the simulation mesh. Also, due to the small size of the inter-fibre bonded area and the difficulty in measuring the force components of an individual bond, the behaviour of the inter-fibre bond was less studied in the literature.

In this work, FE simulations were performed to study the pre-failure behaviour of an inter-fibre bond as well as the bulk properties of paper. In the simulations, actual morphology of NBSK fibres was used to form the 3D mesh for the simulations. In the first part, seven sets of NBSK fibres were used to perform peeling simulations to study the effect of the morphological characteristics of the fibres such as length and diameter on the behaviour of the bond. In these simulations, a breakable cohesive definition in Abaqus™ software was used to form the inter-fibre bond between the fibres. In the second part, tensile strength simulations were performed to simulate the response of a network of NBSK fibres to a uniaxial deformation. An artificial fibre generation code was used to place the fibres with a random position and orientation in the simulation geometries. The morphology of the actual papermaking fibres was used to simulate the behaviour of the geometries with various hardwood/softwood mixtures. Based on the results of these simulations, the effect of the basis weight, the length and diameter of the fibres, and the mixture of hardwood and softwood fibres were studied to determine their effect on the strength of paper. For comparison purposes, tensile strength simulation of a geometry that was formed with simple cylindrical fibres was also performed to show the effect of the actual morphology of the fibres in simulating the behaviour of paper. Finally, the tensile strength simulations were benchmarked by comparing the simulation results with the results of the experimental tensile strength tests that were performed on the actual paper handsheets that were formed in UBC Vancouver campus. The capabilities and limitations of the simulations described and discussed in chapters 4-6 are summarized in sections 6.1 and 6.2 respectively. The recommendations for future works are also listed in section 6.3.

6.1 Capabilities and findings of the simulations

Simulations of the peeling of an individual inter-fibre bond

1. Cohesive behaviour: With the cohesive behaviour definition in Abaqus software, experimental results can be reproduced, which significantly reduces the time and cost of the study. The cohesive behaviour definition can be used to mimic inter-fibre bonds in the FE simulation of the mechanical behaviour of paper. However, it requires extensive work to define a set of local contact surfaces for each pair of fibres. This is difficult for samples with higher basis weights.
2. Morphology of the fibres: This work studied the effect of the morphological characteristics of NBSK fibre on the behaviour of an individual inter-fibre bond. The fracture force and dissipated energy of the inter-fibre bond in paper is affected by the morphological characteristics of the fibres such as length, diameter, and moment of inertia. These parameters can be discussed by studying the effect of the bending stiffness of the top fibre on the peeling strength calculations of an individual inter-fibre bond between a pair of fibres.
   - Beside the strength of the bond, bending stiffness of the top fibre is the parameter that controls the behaviour of the inter-fibre bond.
   - Results of the FE simulations showed that relatively longer fibres with a relatively smaller moment of inertia decreases the bending stiffness of the fibre. Therefore, a relatively lower peeling force and dissipated energy was seen in the simulations.

Tensile Strength Simulations

1. Using the tensile strength simulation of the network of papermaking fibres, bulk mechanical properties of paper handsheets was calculated. These simulations can replace the experimental tests of the strength of paper, reducing the cost and time that needs to be spent on the tests.
2. Using the actual geometry of the papermaking fibres, simulation geometries with various hardwood/softwood mixtures can be produced. These simulations showed the effect of the fibres mixture on the mechanical properties of paper without producing any paper samples.
3. A random network generation script was written for this thesis. This script is able to form simulation geometries by placing the fibres with a random orientation and random position

sequentially in a blank volume. The positions and orientation formed by this script can be used to form simulation geometries with different types of fibres/ and shapes.

4. The results of the tensile strength simulations showed that the tensile index of low density paper samples is dependent on the mechanical characteristics of the fibres as well as the geometrical properties of the network of fibres. The effect of these geometrical properties are listed below:
   - Basis weight: The simulation results showed that the tensile index of the handsheets with a relatively higher basis weight is lower than the geometries with lower basis weights. While the increase in the basis weight of the geometry increased the fracture force of the samples, it was shown that the inverse effect of the basis weight has a significant effect on the tensile index of the samples.
   - Morphology of the papermaking fibres: A comparison between the results of the tensile strength simulation with the actual morphology of the NBSK fibres and a similar simulation with the cylindrical fibres showed that the simulations with the simplified fibres, such as cylindrical results, lead to lower estimation of the actual bulk properties of paper. The results of the simulations showed that any simulation of the strength of paper that is performed based on a geometry of the simplified fibres cannot be considered as a true estimate of the properties of paper unless validated with the experimental results.
   - Elastic modulus of the fibre: In this thesis, the results of the simulation of the tensile strength of a simulation geometry with three different fibre's elastic modulus values was presented. Based on the simulation results, it is shown that tensile index of the geometries is linearly dependent to the elastic modulus of the fibres.
   - Mixture of softwood and hardwood fibres: The effect of the mixture of hardwood and softwood fibres on the strength of paper was studied in this thesis. The tensile index of the simulation geometries with various mass percentage of hardwood fibres were simulated. The results of the simulations showed that the tensile index of the geometry was decreased when the mass percentage of hardwood fibres was decreased.
   - A comparison between the results of the tensile strength simulations and the results of the experimental tests on the paper handsheets showed a good agreement between the simulation results and actual properties of paper. Also, a comparison between the

results of the simulations of low density simulation geometries and tensile strength tests of high density paper handsheets showed that the proposed simulations were able to estimate the tensile index of paper within a good range compared to the experimental test results.

6.2 Limitations

Simulations of the peeling of an individual inter-fibre bond

1. Although the simulation results showed the effect of the morphology of the fibres on the strength of the bond, only the elastic properties of the inter-fibre bond were considered in the peeling simulations.
2. The peeling behaviour of an individual inter-fibre bond in the literature has been described by the delamination of the fibre and the failure of the micro-bonded areas. However, using the cohesive behaviour in Abaqus, the failure of the bond can only be simulated with a stress criterion. Using the cohesive behaviour in Abaqus, the delamination and peeling behaviour of the bonded fibres cannot be simulated completely.
3. The behaviour of the bond was simulated using a breakable cohesive behaviour in Abaqus software. Since the initiation of damage of the bond was defined based on a stress criterion, the behaviour of the bond was influenced by the stress state of the fibre.
4. Since the bond was simulated in Abaqus software, the effect of the bonded area on the strength of the bond was not considered.
5. The material properties of the fibres were defined based on a previous study in the literature. The fibres were supposed to have transversely isotropic elastic modulus with a relatively larger elastic modulus in the length direction.

Tensile Strength Simulations

1. The compression simulations were performed to compress the generated simulation geometries; however, these simulations were limited by the size of the mesh, as coarser mesh could create negative volume error when the fibres are severely compressed and stop the simulation.
2. Although the mesh size of the fibres was increased to reduce the calculation cost of the simulations, the highest basis weight that could be reached for the simulation geometries was 18.2 g/m^2. Larger simulation geometries would include more fibres and require more physical memory and processors.
3. Although the hardwood/softwood mixture geometries that were used for the tensile strength simulations were formed based on various mass percentages of hardwood fibres, the basis weight of the geometries were not constant.
4. Due to the contact definition in Abaqus software, the inter-fibre bonds in the simulation geometries were formed by defining local contact surfaces between the fibres that were closer than the defined vicinity. Although bonded were defined between the fibres in the tensile strength simulations. The bonds were supposed to be fully bonded contacts between the fibres.

6.3 Recommendations for future work

Based on the above discussion, it can be concluded that the numerical simulations that were presented in chapter 4 and 5 were able to predict the bulk mechanical behaviour of paper as well as the pre-failure behaviour of an individual inter-fibre bond. The results of the simulations also showed the effect of the morphological properties of the NBSK fibres, such as length and diameter, on the mechanical behaviour of the inter-fibre bond and the tensile index of paper. This thesis is the first attempt to simulate the mechanical behaviour of paper based on the actual morphology of papermaking fibres. The simulation geometries that were used in the second part of this thesis were formed based on the 3D mesh of the geometry of NBSK fibres that were scanned from actual paper handsheets. The results of the simulations provide a new insight into the mechanical behaviour of paper; however, the following improvements can be added:

Simulations of the peeling of an individual inter-fibre bond

1. A pressure based behaviour could be used to simulate the elastic and plastic deformation of the inter-fibre bond in the peeling simulations. The bond could be defined as a general contact between the fibres in Abaqus software to automatically generate a contact surface between the fibres.
2. Peeling simulations could include micro-mechanical characteristics of the bond, such as delamination of the bonded section of the fibre and the micro failures of the inter-fibre bond.
3. The peeling simulations could be performed to study the behaviour of the bond various physics that has been proposed in the literature to define the mechanics of the inter-fibre bond, such as Van der Waals force, mechanical inter-lock, and hydrogen bond.
4. Local mesh refinement of fibres in the bonding area would increase the simulation accuracy.

Tensile Strength Simulations

1. The proposed methodology for the tensile strength simulation needs to be developed further for robust use, however, requires significant computational cost.
2. Tensile strength simulations of the geometries with higher basis weights can be performed to validate the results of the proposed simulation methodology with experimental tensile strength test results.
3. Tensile strength simulations of the softwood/hardwood mixed geometries with a fixed basis weight can show the effect of the mixture of fibres without the effect of basis weight.
4. An automated algorithm to form the inter-fibre bonds can help to form the network of fibre in the simulation geometries in an easier way.
5. The cohesive contact definition can be used to define the inter-fibre bonds in the tensile strength simulation geometries, forming a more realistic approximation of the geometry of paper.
6. The results of the simulations can be used to develop a constitutive behaviour model for the mechanical behaviour of paper; however, more simulations should be performed to include the effect of all of geometrical and mechanical characteristics of NBSK fibres.

References

1 Hiltunen, E. (2003). On the beating of reinforcement pulp Helsinki University of Technology.

2 Alava, M., & Niskanen, K. (2006). The physics of paper. Reports on Progress in Physics, 69(3), 669.

3 Andersson, M., Persson, L., Sjöholm, M., & Svanberg, S. (2006). Spectroscopic studies of wood-drying processes. Optics Express, 14(8), 3641-3653.

4 Nanko, H., Button, A., & Swann, C. E. (2005). The world of market pulp WOMP LLC.

5 Brebbia, C. A. (1985). Finite element systems: A handbook Springer.

6 Wilbrink, D. (2011). Modelling the in-plane mechanical behaviour of paper.

7 Heyden, S. (2000). Network modelling for evaluation of mechanical properties of cellulose fibre fluff Lund University.

8 Karlsson, H. (2007). Some aspects on strength properties in paper composed of different pulps.

9 Banik, G., Brückle, I., Daniels, V., Fischer, S., Keller, S. W., Kosek, J. M., Wegele, G. (2011). Paper and water: A guide for conservators Butterworth-Heinemann Oxford.

10 Karlsson, M., & Oyj, M. (2000). Book 9: Papermaking Part2, drying. Papermaking Science and Technology.Finland: Finnish Paper Engineers Association and TAPPI,

11 Niskanen, K., & Alava, M. J. (1994). Planar random networks with flexible fibers. Physical Review Letters, 73(25), 3475.

12 Retulainen, E. (1997). The role of fibre bonding in paper properties Helsinki University of Technology, Department of Forest Products Technology, Laboratory of Paper Technology= Teknillinen Korkeakoulu, Puunjalostustekniikan laitos, Paperitekniikan laboratorio.

13 Torgnysdotter, A., & Wågberg, L. (2003). Study of the joint strength between regenerated cellulose fibres and its influence on the sheet strength. Nordic Pulp & Paper Research Journal, 18(4), 455-459.

14 CHINGA-CARRASCO, G. (2009). Exploring the multi-scale structure of printing paper–a review of modern technology. Journal of Microscopy, 234(3), 211-242.

15 Sharma, Y. (2014). Automated fibre segmentation in micro CT images of paper.

16 Sharma, Y., Phillion, A., & Martinez, M.High resolution micro CT imaging and 3D image analysis of paper products. 2nd International Congress on 3D Materials Science, 41-46.

17 Sarkanen, K. V., & Ludwig, C. H. (1971). Lignins: Occurrence, formation, structure and reactions. Lignins: Occurrence, Formation, Structure and Reactions.,

18 Yan, D., & Li, K. (2012). Evaluation of inter-fiber bonding in wood pulp fibers by chemical force microscopy. Journal of Materials Science Research, 2(1), p23.

19 http://www.paperonweb.com/paperpro.htm#top1

20 http://aesop-innovation.com/pages/what-is-liquidwood.php

21 Ebeling, K. (1997). Role of softwood fibre form and condition on its reinforcement capability. Wochenblatt Fur Papierfabrikation, 125(16), 757-764.

22 Paavilainen, L. (1993). Importance of cross-dimensional fibre properties and coarseness for the characterisation of softwood sulphate pulp. Paperi Ja Puu, 75(5), 343-351.

23 Paavilainen, L. (1993). Conformability, flexibility and collapsibility of sulphate pulp fibres. Paperi Ja Puu, 75(9-10), 689-702.

24 Salminen, L., Alava, M., Heyden, S., Gustafsson, P., & Niskanen, K. (2002). Simulation of network shrinkage. Nordic Pulp & Paper Research Journal, 17(2), 105-110.

25 Van den Akker, J. (1962). Some theoretical considerations on the mechanical properties of fibrous structures. The Formation and Structure of Paper, 1, 205-245.

26 Hoffman-Jacobsen, P. (1925). A new method of determining of the strength of chemical pulp. Paper Trade Journal, 53(1), 216-217.

27 Van Den, Akker Johannes A. (1950). Creep Testing Apparatus,

28 Van den Akker, J., Lathrop, A., Voelker, M., & Dearth, L. (1958). Importance of fiber strength to sheet strength. Tappi, 41(8), 416-425.

29 Gibbon, E. (1944). Stress/strain curves of paper. Proc.Tech.Section, Paper Makers Assoc.Gt.Britain Ireland, 25, 199-210.

30 Mason, S. (1948). The rheology of paper: A new approach to the study of paper strength. Paper Maker, 53-56.

31 Rance, H. (1948). Pap. makers' assoc. GB Irel., Proc.Tech.Sect, 29, 449.

32 Seth, R. (2004). Understanding sheet extensibility. Annual Meeting-Pulp and Paper Technical Association of Canada, , 90(A) 51-60.

33 Niskanen, K. (1998). Kraft fibers in paper–Effect of beating. Cellucon’98 Conference,

34 Honkasalo, J. (2004). Behaviour of different furnish mixtures in mechanical printing papers Helsinki University of Technology.

35 Görres, J., Amiri, R., Wood, J. R., & Karnis, A. (1996). The apparent density of sheets made from pulp blends. Tappi Journal, 79(1), 179-187.

36 ZHANG, G., & LAINE, J. E. (2002). Chracteristics of the strength properties of a mixture sheet under wet straining drying. Paperi Ja Puu, 84(3), 169-173.

37 I'Anson, S., Sampson, W., & Savani, S. (2008). Density dependent influence of grammage on tensile properties of handsheets. 0826-6220, 34(3), 182-189.

38 Page, D., Seth, R., & Degrace, J. (1979). Elastic-modulus of paper. 1. controlling mechanisms. Tappi, 62(9), 99-102.

39 Cox, H. (1952). The elasticity and strength of paper and other fibrous materials. British Journal of Applied Physics, 3(3), 72.

40 Page, D., & Seth, R. (1980). The elastic-modulus of paper. 2. the importance of fiber modulus, bonding, and fiber length. Tappi, 63(6), 113-116.

41 Lindström, T., Wågberg, L., & Larsson, T. (2005). On the nature of joint strength in paper– A review of dry and wet strength resins used in paper manufacturing. Proc. 13th Fundamental Research Symp,

42 Page, D. (1969). A theory for tensile strength of paper. Tappi, 52(4), 674-&.

43 Ramasubramanian, M., & Perkins, R. (1988). Computer simulation of the uniaxial elastic-plastic behaviour of paper. Journal of Engineering Materials and Technology, 110(2), 117-123.

44 Ramasubramanian, R., & Wang, Y. Y. (1999). Constitutive models for paper and other ribbon-like nonwovens-a literature review. Asme,

45 Xia, Q. S., Boyce, M. C., & Parks, D. M. (2002). A constitutive model for the anisotropic elastic–plastic deformation of paper and paperboard. International Journal of Solids and Structures, 39(15), 4053-4071.

46 Mäkelä, P., & Östlund, S. (2003). Orthotropic elastic–plastic material model for paper materials. International Journal of Solids and Structures, 40(21), 5599-5620.

47 Heyden, S., & Gustafsson, P. (2001). Stress–strain performance of paper and fluff by network modelling. 12th Fundamental Research Symposium, Oxford,

48 Lavrykov, S., Lindström, S., Singh, K., & Ramarao, B. (2012). 3D network simulations of paper structure. Nordic Pulp and Paper Research Journal, 27(2), 256.

49 Bronkhorst, C. (2003). Modelling paper as a two-dimensional elastic–plastic stochastic network. International Journal of Solids and Structures, 40(20), 5441-5454.

50 Rigdahl, M., Westerlind, B., & Hollmark, H. (1984). Analysis of cellulose networks by the finite element method. Journal of Materials Science, 19(12), 3945-3952.

51 Perkins, R. (1980). Proceedings of the conference of paper science and technology: The cutting edge. Institute of Paper Chemistry, Appleton, , 89.

52 Jangmalm, A., & Östlund, S. (1995). Modelling of curled fibres in two-dimensional networks. Nordic Pulp & Paper Research Journal, 10(3), 156-161.

53 Astrom, J., & Niskanen, K. (1991). Simulation of network fracture. Proceedings of the 1991 International Paper Physics Conference, 31-47.

54 Åström, J., & Niskanen, K. (1993). Symmetry-breaking fracture in random fibre networks. EPL (Europhysics Letters), 21(5), 557.

55 Åström, J., Saarinen, S., Niskanen, K., & Kurkijärvi, J. (1994). Microscopic mechanics of fiber networks. Journal of Applied Physics, 75(5), 2383-2392.

56 Niskanen, K. (1993). Strength and fracture of paper. Products of Papermaking: Transactions of the Tenth Fundamental Research Symposium, 2, 641-725.

57 Karakoç, A. (2015). A fiber network model to understand the effects of fiber length and height on the deformation of fibrous materials.

58 Deng, M., & Dodson, C. T. J. (1994). Paper: An engineered stochastic structure Tappi.

59 Kähkönen, S. (2003). Elasticity and stiffness evolution in random fibre networks University of Jyväskylä.

60 Räisänen, V., Alava, M., Nieminen, R., & Niskanen, K. (1996). Elastic-plastic behaviour in fibre networks. Nordic Pulp and Paper Research Journal (Sweden),

61 Borodulina, S., Kulachenko, A., Galland, S., & Nygårds, M. (2012). Stress-strain curve of paper revisited. Nordic Pulp and Paper Research Journal, 27(2), 318.

62 Mark, R. E., & Borch, J. (2001). Handbook of physical testing of paper CRC Press.

63 Hirn, U., & Schennach, R. (2015). Comprehensive analysis of individual pulp fiber bonds quantifies the mechanisms of fiber bonding in paper. Scientific Reports, 5

64 Holmberg, M., Berg, J., Stemme, S., Ödberg, L., Rasmusson, J., & Claesson, P. (1997). Surface force studies of Langmuir–Blodgett cellulose films. Journal of Colloid and Interface Science, 186(2), 369-381.

65 Notley, S. M., Pettersson, B., & Wågberg, L. (2004). Direct measurement of attractive van der waals' forces between regenerated cellulose surfaces in an aqueous environment. Journal of the American Chemical Society, 126(43), 13930-13931.

66 Fischer, W. J., Hirn, U., Bauer, W., & Schennach, R. (2012). Testing of individual fiber-fiber joints under biaxial load and simultaneous analysis of deformation. Nord Pulp Pap Res J, 27(2), 237-244.

67 Persson, K. (2000). Micromechanical modelling of wood and wood fiber properties. Department of Mechanics and Materials, Structural Mechanics, LUND University, Sweden,

68 Hägglund, R., & Isaksson, P. (2008). On the coupling between macroscopic material degradation and interfiber bond fracture in an idealized fiber network. International Journal of Solids and Structures, 45(3), 868-878.

69 Magnusson, M. S. (2011). Inter-fibre bond strength and combined normal and shear loading. Progress in Paper Physics Seminar, Graz, Austria, September 5-8, 2011,

70 Schmied, F. J., Teichert, C., Kappel, L., Hirn, U., Bauer, W., & Schennach, R. (2013). What holds paper together: Nanometre scale exploration of bonding between paper fibres. Scientific Reports, 3

71 Magnusson, M. S., & Östlund, S. (2013). Numerical evaluation of interfibre joint strength measurements in terms of three-dimensional resultant forces and moments. Cellulose, 20(4), 1691-1710.

72 Reme, P., & Kure, K. (2003). Stereo images as a tool to study paper surface topography. Journal of Pulp and Paper Science, 29(3), 86-89.

73 Hanley, S. J. (1995). Application of atomic force microscopy to cellulose, wood, kraft pulp fibres and paper

74 I'Anson, S. J., Sampson, W. W., & Savani, S. (2008). Density dependent influence of grammage on tensile properties of handsheets. 0826-6220, 34(3), 182-189.